GRAPHENE AND ITS DERIVATIVES: A REVIEW

AND GRAPHENE GROWTH ON INSULATING SUBSTRATES VIA NICKEL DIFFUSION

by

JULIET L DEFINO

A thesis submitted to the

Graduate School-New Brunswick

Rutgers, The State University of New Jersey

in partial fulfillment of the requirements

for the degree of

Master of Science

Graduate Program in Materials Science and Engineering

written under the direction of

Dr. Manish Chhowalla

and approved by

_____

_____

_____

New Brunswick, New Jersey

May 2012

ABSTRACT OF THE THESIS

Graphene and Its Derivatives: A Review

and Graphene Growth on Insulating Substrates via Nickel Diffusion

By JULIET L DEFINO

Thesis Director:
Dr. Manish Chhowalla

This thesis is composed of a review on the rapidly growing field of graphene research and an experimental investigation of a synthesis method to produce high quality graphene on insulating substrates via diffusion of carbon through nickel. The history, synthesis, characterization, properties, and applications of graphene and its derivatives are comprehensively discussed in the review. Historical milestones span the first theoretical publication on graphene in 1947 to K. S. Novoselov and A. K. Geim's groundbreaking discovery in 2004. A variety of physical and chemical synthesis techniques have been discovered, each with their own advantages and disadvantages. Several forms of microscopy and spectroscopy have been utilized to realize the material's exceptional structural, electronic, optical, mechanical, and thermal properties. Together, these qualities have justified graphene thin films' capability to be integrated into a widespread collection of electronic devices.

The objective of the experimental section is to explore a novel synthesis procedure entailing the spin coating of a carbon solution onto a thermally evaporated 40 nm layer of nickel on a SiO_2/Si substrate. The samples were annealed at 50°C, 100°C, 150°C, 200°C, or 400°C for 4 hours to initiate the diffusion of carbon through the metal and deposition onto

the substrate. Etching of the metal and excess carbon source material took place in a 5:1 HCl and HNO_3 solution. Distinctive D, G, and 2D peaks at around 1350 cm^{-1}, 1580 cm^{-1}, and 2700 cm^{-1} in the Raman spectra indicated the material was graphitic, but an increasing slope in the Raman shift suggested that the nickel layer was still present. 2D/G integrated intensity area ratios showed a peak somewhere between 100° and 150°C, which implied an ideal growth temperature within that range. D/G area ratios exhibited unexpected and questionable behavior. Despite these inconclusive results, a recent paper by Kwak et al proposing a similar growth method did in fact prove that high quality few layer graphene sheets can be successfully produced via this technique. A brief review of that paper is included.

Acknowledgement and Dedication

This thesis is dedicated to my mother Terri Gilroy Defino, my father Robert Defino, and the rest of my family for their endless love and support, and my friends Karen Piatek, Kristina Ruskuls, Laura Racop, and Anna Lempart for steadfastly being there for me over the last two years through thick and thin. I couldn't have done this without all of you.

I would like to acknowledge my advisor and the entire Nano-materials & Devices group, especially Dr. Hisato Yamaguchi, Dr. Damien Voiry, Ethan Cheng, Sarah Snyder, Austin Geary, and Jaesung Kim, who participated in this project with me. A special thanks goes out to Rajesh Kappera, who was not only a great co-worker, but also a good friend throughout the process of writing this thesis.

Table of Contents

List of Illustrations

Introduction

To the untrained eye, a single atomic plane of sp^2 carbon atoms may come off as a rather simple and unimpressive material, but looks can be deceiving. This carbon allotrope, known as graphene, has garnered astronomical attention within the last decade for its phenomenal, one of a kind qualities and vast potential for implementation in a myriad of technological applications. It can be synthesized using a variety of techniques that employ bulk graphite and other readily available and inexpensive carbon materials as sources. Due to its two-dimensionality and unique chemical makeup, graphene exhibits remarkable structural, electronic, optical, mechanical, and thermal properties. These qualities make it a prime contender to replace such conventional materials such as silicon in transistors and indium tin oxide in transparent electrodes. Research in the field of graphene has grown exponentially in recent years, all a result of the escalating anticipation to uncover this extraordinary material's true potential.

The following thesis is comprised of two major parts: 1) an up to date review on the field of graphene research and 2) a proposal for a novel synthesis route of scalable, high quality graphene thin films for use on an industrial level. The review covers the history, synthesis, characterization, properties, and applications of graphene and its derivatives. It elaborates on the potential graphene has to revolutionize the field of nanotechnology and electronic devices, and also explains why graphene has yet to break into the industrial world. The experimental section investigates a new technique for manufacturing graphene via the diffusion of carbon through nickel onto an insulating substrate. This area of research is worthwhile due to its capacity to be developed into a large-scale, substrate independent production method of high quality graphene sheets, which could help ease graphene into position for widespread industrial applications.

Part I – Graphene and Its Derivatives: A Review

Part I, Section I – History

Graphite, a naturally occurring allotrope of carbon, has been well known throughout history for its easily cleavable, flake-like nature and ability to be implemented in a wide variety of uses, ranging from writing tools to dry lubricant. Its two-dimensional counterpart, however, had long been believed to be unable to exist independently and thus was only speculated on in theory [1, 2]. These theories claimed that purely 2-D crystalline planes of atoms were thermodynamically unstable and would disassemble into islands or decompose if under approximately 20 nm, which consisted of several dozens of layers [1-3]. This idea was reinforced by experimental observation, since at the time freestanding 2-D crystals had not successfully been isolated and were only discernible when accompanied by a much larger 3-D base [1, 2].

Among the myriad of hypothetical 2-D materials, planar sheets of carbon atoms attracted particular interest because of their advanced theoretical electronic capabilities [2, 3]. A two-dimensional single graphitic layer is composed of carbon atoms arranged in a honeycomb-like lattice with a carbon-carbon bond length of 0.142 nm. It is the essential building block of all other carbon allotropes (zero-dimensional fullerenes, one-dimensional nanotubes, and three-dimensional graphite) as depicted in Figure 1. The earliest speculation on this unique material's electronic properties was published by P. R. Wallace in 1947. He surmised an analytical term for the electronic band structure due to the substantial delocalization of all the carbon-carbon π bonds on either side of the atomic plane [3]. This in turn led to further predictions of exceptional near-relativistic phenomena that could occur within this thus far elusive material [2, 3].

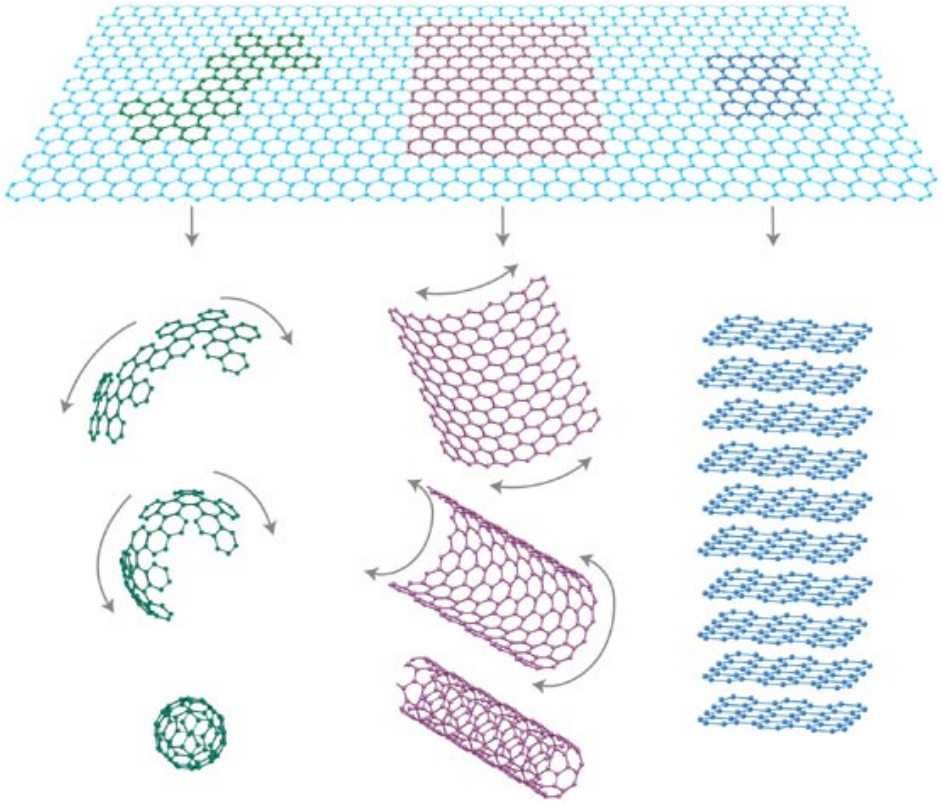

Figure 1: A two-dimensional monolayer of carbon atoms, the "mother of all graphitic forms", is the basis of carbon allotropes of all other dimensionalities: 0-D fullerenes, 1-D nanotubes, and 3-D graphite. Reprinted by permission from MacMillan Publishers Ltd: Nature Materials [2], copyright 2007.

These predictions were bolstered by experimental evidence in the 1960s during studies of graphite intercalation compounds. Intercalation is the process of introducing large molecules in between the individual atomic layers of a bulk material. It was discovered that basal plane conductivity readings of the intercalated materials were much higher than that of the pristine graphite [1]. Upon attempts to isolate graphite monolayers by chemically removing the intercalated molecules, a blend or "slurry" of restacked and scrolled layers was produced and no individual 2-D crystals were ever able to be extracted [1, 2, 4]. Unfortunately, the unmanageability of these graphitic slurries has rendered them virtually useless in the pursuit of planar carbon monolayers [2].

Attempts to grow single layers of graphite were also made, including the same method for producing carbon nanotubes, thermal decomposition of SiC, and chemical vapor deposition of hydrocarbon gases on metal substrates. While these techniques did successfully yield thin film multi-layer graphite, no monolayers were observed [1, 2]. During this time, the term "graphene" was officially coined in 1994 by H. P. Boehm et al in a recommendation article to the IUPAC. The authors reasoned that the term "graphite" was only appropriate for materials that induce a modulation of the *hk* reflections in X-ray diffraction and single graphitic layers did not fall into this classification. They stated that the suffix –*ene* is utilized for fused polycyclic aromatic hydrocarbons and since the planar, crystalline arrangement of carbon atoms is the base component of graphite, it should be deemed graphene [5].

A major breakthrough in the field of graphene occurred in 2004, when K. S. Novoselov and A. K. Geim successfully isolated a single atom thick layer of graphene via mechanical exfoliation [1-4, 6]. This was accomplished by a rather simple technique: the repetitive peeling of small mesas of highly oriented pyrolytic graphite using adhesive tape, commonly known as the "scotch tape" method. The procedure was both consistent and reproducible, yielding graphene monolayers of up to 10 μm in width and few layer graphene of up to 100 μm [6]. These films were studied and found not only to be continuous and exhibit high quality crystal structure, but also to display remarkable carrier mobilities and concentrations resulting in ballistic transport on submicrometer scales [2-4, 6]. And perhaps the most counterintuitive observation: the 2-D crystals were stable under ambient conditions and did not structurally or electronically degrade over time, in complete opposition to long accepted theory [4].

Within the last decade, research in the field of graphene has experienced boundless growth due to the material's tremendous electronic characteristics [1, 3]. Topics include

regulation of the number of layers grown, functionalization of the material, and potential for electronic applications. Undoubtedly, this can be attributed to K. S. Novoselov and A. K. Geim's high impact discovery in 2004, which ultimately awarded them the 2010 Nobel Prize in Physics [3]. A graphical illustration of the definitive influence of this publication is portrayed in Figure 2.

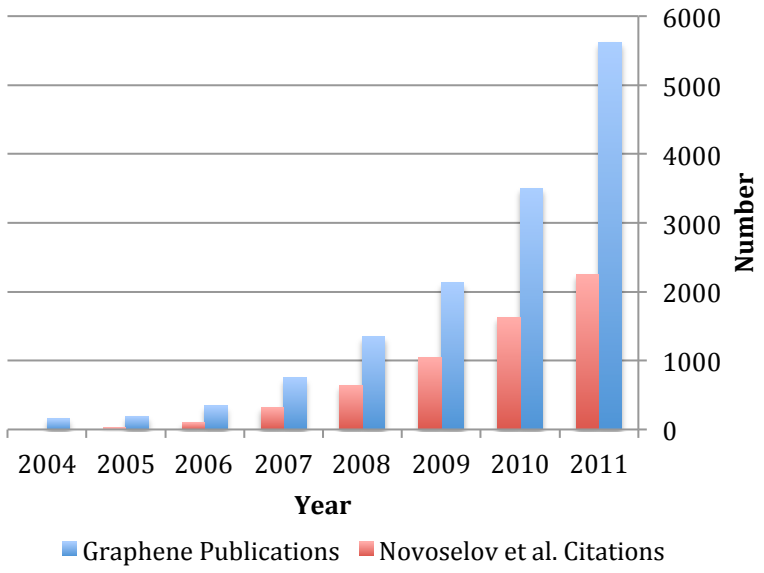

Figure 2: Graphical depiction of the recent surge in graphene related research. Both the number of overall publications on graphene and the number of citations of Novoselov et al's 2004 *Science* article are plotted per year to show the impact this paper has had on the field. Data sourced from Web of Knowledge.

Part I, Section II – Synthesis

Mechanical Exfoliation/Cleavage

As detailed in the previous section, single layers of graphene were first attained in 2004 via the "scotch tape" method, which entailed the physical cleavage of highly oriented pyrolytic graphite (HOPG) [6]. A photograph of this procedure can be found in Figure 3. While this technique does provide continuous, high quality material conducive for implementation in experimental devices and measurements, it is by no means a valid process for large-scale production. Thus, methods of mechanical exfoliation in solutions where the material's chemical structure is left unaltered became of interest [1].

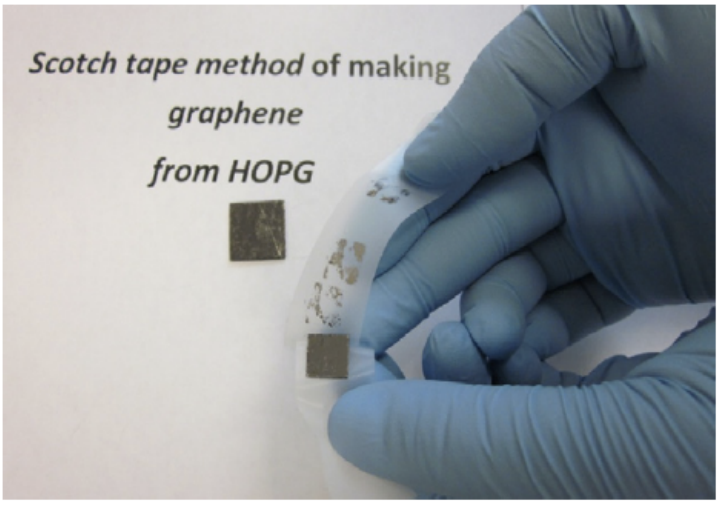

Figure 3: "Scotch tape" method of mechanically exfoliating graphene monolayers from HOPG. Reprinted from [1] with permission from Elsevier.

One example of this is the use of *N*-methyl-pyrrolidone. This process utilizes the similar surface energies of *N*-methyl-pyrrolidone and graphite to expedite the exfoliation process, which is then followed by vaporization of the solution in order to deposit the exfoliated graphene. Drawbacks to mass production by means of this approach are *N*-methyl-pyrrolidone's high cost and elevated boiling point [7]. Another tactic is the dispersion of bulk graphite in a surfactant-water solution via ultrasonication. The

surfactant forms micelles that envelope the graphene layers, preventing aggregation. Two surfactants that have been experimented with are sodium dodecylbenzene sulfonate (SDBS) and sodium cholate (SC) [8, 9].

Also discussed in Section I were graphite intercalation compounds. While many attempts to attain graphene from intercalated materials resulted in graphitic slurries with no further application, these compounds have been successfully employed to generate expanded graphene, or EG. In this variation of graphene synthesis, an ultrasonic solvent (ideally, concentrated sulfuric acid) is introduced in between individual flakes. The subsequent solution is rinsed with water and dried, resulting in aggregated layers with molecules of the solvent sandwiched within. Upon heating, the interspersed solvent releases a gas that separates the graphene, giving rise to EG [1].

Chemical Vapor Deposition

Unlike mechanical exfoliation, which is considered a "top down" synthesis approach, chemical vapor deposition, or CVD, is a "bottom up" method. This means that instead of taking a bulk substance and dividing it until a single 2-D layer is achieved, one starts on the atomic level and grows the material, essentially, from the bottom up. Thermal CVD is the process during which carbon from a hydrocarbon gas (most often methane) or a solid source is adsorbed onto the surface of a metal substrate under high temperatures, generating graphene layers. An example of graphene grown via thermal CVD is presented in Figure 4. There are two general types of CVD substrates: high carbon solubility metals and low carbon solubility metals [1].

During CVD onto high carbon solubility metals, such as nickel and cobalt, the carbon begins to diffuse into the surface of the metal and upon quenching, precipitates out of the substrate, forming thin graphene films. Product thickness and quality depend on the

cooling rate and the amount of carbon dispersed into the metal [10]. The resultant films are composed of three to eight layers, and exact thickness regulation during synthesis is challenging [1]. On low carbon solubility metals, like copper, the carbon accumulates into nuclei on the surface of the metal that propagates outward until they come into contact with other graphene islands. Substrate coverage is dependent on annealing temperature, the hydrocarbon gas flow rate, and the gas partial pressure [11]. Universally, graphene films grown on Cu are monolayers or bilayers, thus thickness control is not an issue [1]. The low solubility of the metal has been credited to making the process "self-limiting", meaning it will terminate once coverage has reached 100%, which not only ensures full substrate coverage but also prevents undesirable thick graphene growth [12].

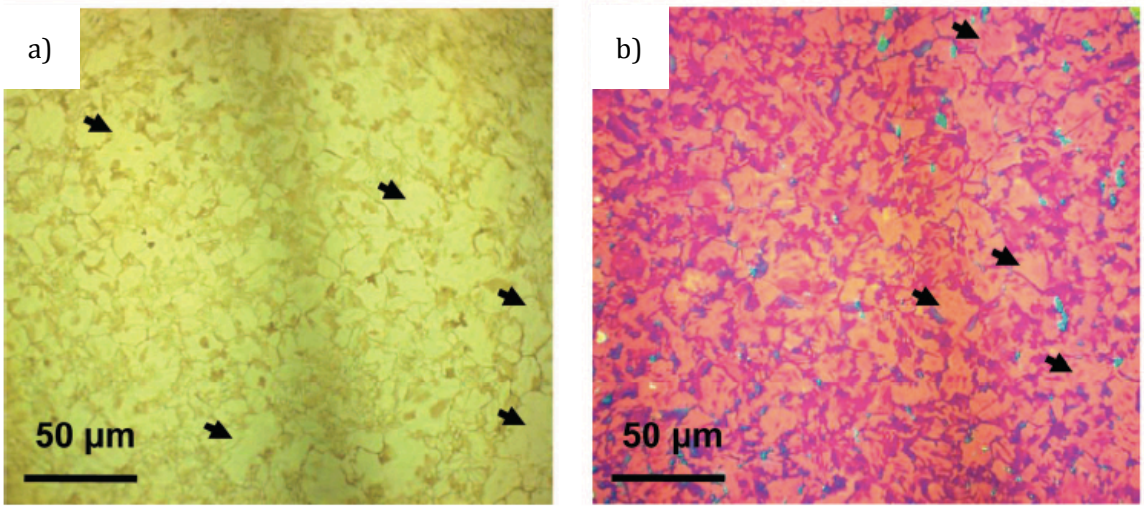

Figure 4: a) Optical image of a Ni film with graphene grown on its surface. b) Optical image of the same graphene film transferred to a Si_2O/Si substrate. Black arrows indicate areas of monolayer and bilayer graphene that coincide with the Ni grain boundaries. Reprinted with permission from [10]. Copyright 2009 American Chemical Society.

Another CVD technique is plasma-enhanced chemical vapor deposition, abbreviated PECVD. This variation boasts a lower temperature and shorter growth time than thermal CVD and has the capability of generating graphene on any substrate that can withstand the deposition temperature. The synthesis mechanism consists of a coordinated

recombination of carbon radicals within plasma and results in the deposition of graphene layers in a vertical orientation to the substrate [13].

Thermal Decomposition/Epitaxial Growth

Along with CVD, thermal decomposition and epitaxial growth are also "bottom up" methods of graphene fabrication [1]. Thermal decomposition entails the annealing of a (0001) crystal face of a SiC wafer under ultrahigh vacuum (UHV) conditions. The heating causes the silicon to sublimate, leaving behind highly structured carbon atoms that subsequently bond with each other to create graphene layers. The thickness and continuity of the graphene growth depends on both the annealing time and temperature [14]. Advantages of this technique are its potential applicability to large-scale production and the fact that the graphene is already on a SiC substrate for immediate implementation in the semiconductor industry. However, disadvantages include inconsistencies in graphene thickness and coverage of the substrate and the dependence of product quality on whether growth initiates from a silicon or a carbon crystal face. It has been shown that graphene layers formed on a carbon foundation demonstrate abnormal stacking rotation, which detrimentally affects material properties [1].

A similar approach to thermal decomposition is the epitaxial growth of graphene on various metals. The most prominent substrate is ruthenium. Sparse carbon nucleation is initiated on the (0001) crystal face of the metal, which propagates into linear regions across the substrate. The first graphene layer has been found to be strongly bound to the ruthenium, while the second layer is virtually detached, displaying very similar properties to freestanding graphene [15]. Other metal substrates used for epitaxial growth include nickel, cobalt, iridium, and platinum [1].

Chemically Derived Graphene

An alternative synthesis technique is the chemical exfoliation of graphene, producing what is known as chemically derived graphene, abbreviated CDG. The fabrication of CDG involves the following steps: oxidation of bulk graphite, exfoliation and aqueous dispersion of graphene oxide (GO) platelets and sheets, reduction of the GO into reduced graphene oxide (rGO), and thin film deposition. The overall scheme is depicted in Figure 5. Graphite oxide is created via the addition of bulk graphite in one or more concentrated acids in the presence of an oxidizing agent [16]. The oxidation step introduces covalent oxygen functional groups, such as carboxyl groups and ethers, to the carbon basal planes [17], as displayed in Figures 6 and 7. Once oxidized, the material will readily go into solution in an aqueous environment and delaminate into GO platelets and monolayers, which remain dispersed due to the polarized functional groups. This poses a huge advantage in manageability over pristine graphene, which is hydrophobic and tends to aggregate in solution [16].

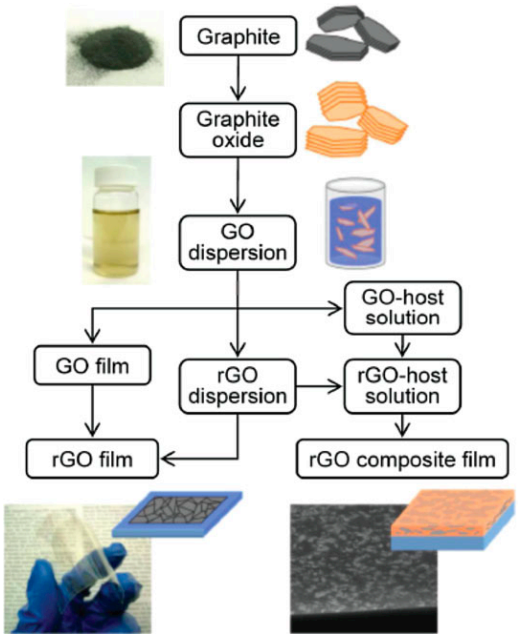

Figure 5: Fabrication scheme of rGO thin films via the oxidation and exfoliation of graphite. Reprinted by permission from John Wiley & Sons, Inc.: Advanced Materials [16], copyright 2010.

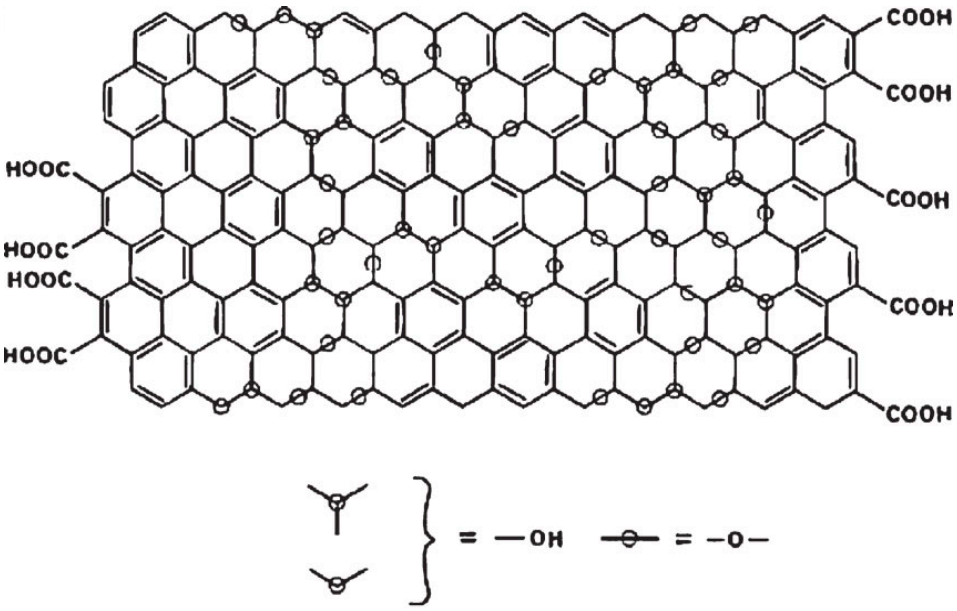

Figure 6: Molecular structure of a monolayer of graphene oxide. Reprinted with permission from [17]. Copyright 1998 American Chemical Society.

A significant consequence of oxidation, however, is a complete transition in the electronic properties of the material, from a nearly relativistic conductor to an insulator. This effect is alleviated by a subsequent reduction of GO into rGO. Transmission electron microscope images of the atomic structure of rGO can be found in Figure 8. Reduction of the GO layers can be achieved through a variety of techniques, but the most widely used are chemical reduction and thermal reduction. Two of the most prominent chemical reducing agents are hydrazine (N_2H_4) and sodium borohydrate ($NaBH_4$). Once the GO solution has been reduced, many thin film deposition methods can be employed, such as drop-casting, dipcoating, spraying, spin-coating, electrophoresis, and transfer via vacuum filtration. Parameters including the uniformity, morphology, thickness, and surface coverage of the film are dependent on the method and conditions used. Most often, vacuum filtration is used for its high degree of control regarding the film characteristics [16].

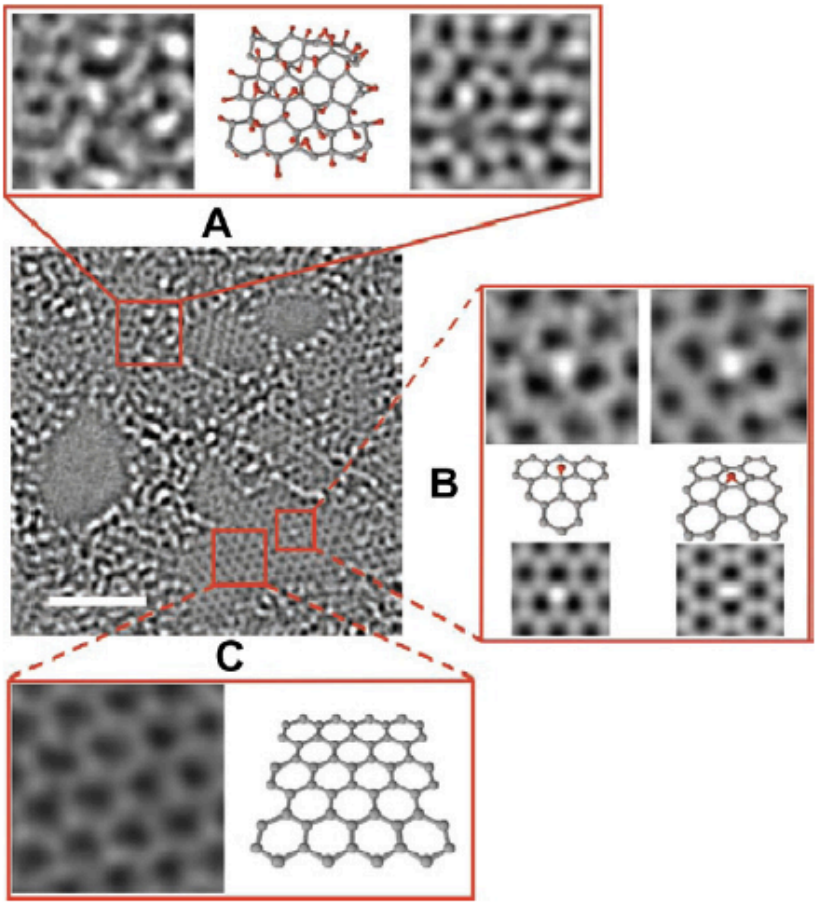

Figure 7: High resolution TEM image of a monolayer of GO. Expansion A shows an enlargement of an oxidized area within the atomic structure and a "ball and stick" simulation of how this area may be arranged with oxygen atoms in red. Expansion B shows an enlargement and subsequent simulation of an area with a single oxygen functionalization group and its transition from a hydroxyl position to an epoxy site. Expansion C shows a pristine area of the material. Reprinted by permission from John Wiley & Sons, Inc.: Advanced Materials [18], copyright 2010.

While reduction restores the material's ability to conduct, presently utilized procedures do not fully remove all of the oxygen functional groups from the carbon basal plane. Thus, the charge transport properties are hindered and the relativistic nature of pristine graphene is not re-established. However, what makes CDG attractive is the ease of its synthesis, manageability, and incorporation into electronic devices via the utilization of thin film techniques [16].

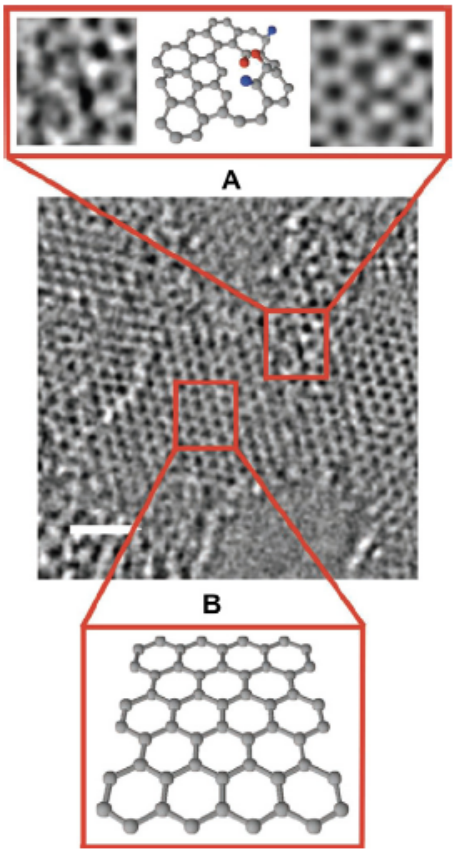

Figure 8: High resolution TEM image of a monolayer of rGO. Expansion A shows an enlargement of an area where functional groups remain within the atomic structure and a "ball and stick" simulation of how this area may be arranged with oxygen atoms in red and nitrogen atoms in blue. Expansion B shows a pristine area of the material. Reprinted by permission from John Wiley & Sons, Inc.: Advanced Materials [18], copyright 2010.

Graphene Nanoribbons

Unlike the previously discussed thin films that are 2-D and continuous, graphene nanoribbons, or GNRs, are quasi 1-D strips of graphene with a width of only a few nanometers [12], as pictured in Figure 9. The motivation behind development of GNRs and their synthesis techniques is the necessity to introduce a band gap into graphene in order to make it pertinent for use in the semiconductor industry. Conventional 2-D graphene films are zero band gap semiconductors, as will be detailed in Section IV, and thus cannot be implemented into devices as is [6, 12]. The orientation of the GNR edges, either zigzag or

armchair, have an influence on the material's electronic properties and designate it either a semiconductor or a metal [6].

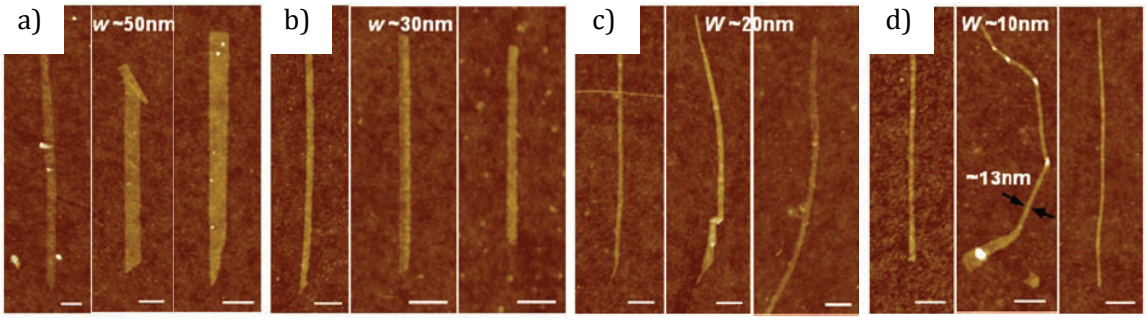

Figure 9: AFM images of GRNs of varying widths: a) ~50 nm, b) ~30 nm, c) ~20 nm, and d) ~10 nm. From [19]. Reprinted with permission from AAAS.

Nanoribbons can be fabricated in a number of ways. The first is electron beam lithography patterning and subsequent etching [12]. There are also several organic synthesis techniques and other chemical routes, including the noncovalent polymer functionalization of thermally exfoliated graphite [19], which was utilized to generate the GNRs in Figure 9. The final method is the unzipping of multi-walled carbon nanotubes (MWCNTs) via chemical oxidation or plasma etching [20]. A progression of this unzipping process can be found in Figure 10.

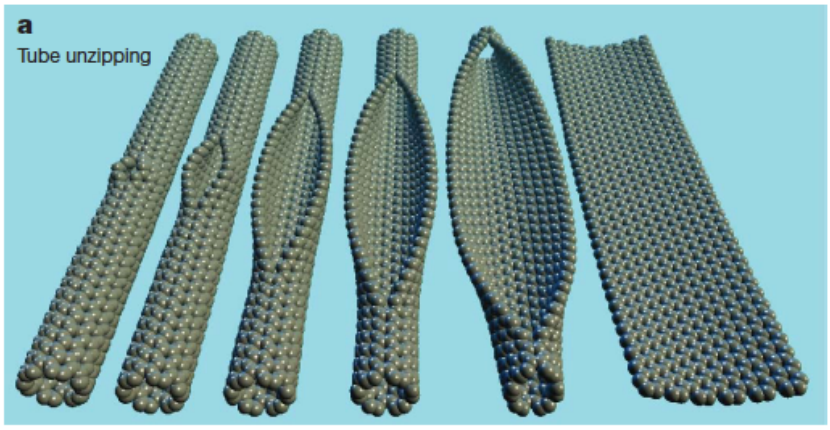

Figure 10: Illustration of the unzipping of MWCNTs into GNRs. Reprinted with permission from Macmillan Publishers Ltd: Nature [20], copyright 2009.

Part I, Section III – Characterization Methods

Several techniques are utilized to study graphene and its derivatives, the most prominent of which will be covered in this section. However, it is first important to note that often a combination of two or more methods are needed for proper characterization.

Optical Microscopy

Optical microscopy, perhaps the cheapest and most readily accessible method of characterization, is especially significant in the study of graphene as it is the only technique with the ability to detect single to few layer films on a large scale [1, 21]. Other methods have such a minute throughput that it is virtually impossible to discover monolayers without previous knowledge of their location, comparable to finding a needle in the "haystack" of thicker graphitic clusters. What makes optical observation so advantageous is a) the ability to physically scan over a specimen at a fast rate and b) the existence of optical interference between the flake and the substrate which enable the material to be visible [21], as evidenced in Figure 11. The explanation behind this phenomenon is presented in the Optical Properties segment of Section IV. In fact, the presence of this interference contrast is credited to being the crucial reason behind K. S. Novoselov and A. K. Geim's 2004 discovery of freestanding graphene monolayers [4].

In order for graphene to be visible however, it does need to be mounted on a certain type of substrate that induces interference [1]. Generally, substrates are a silicon base with a thin layer of a dielectric substance deposited on the surface [1, 21]. The most commonly used materials are SiO_2 and Si_3N_4 and thicknesses are most frequently in the ~300 nm range. Different dielectric thicknesses and light wavelengths are currently being experimented with to determine their impact on optical contrast [1].

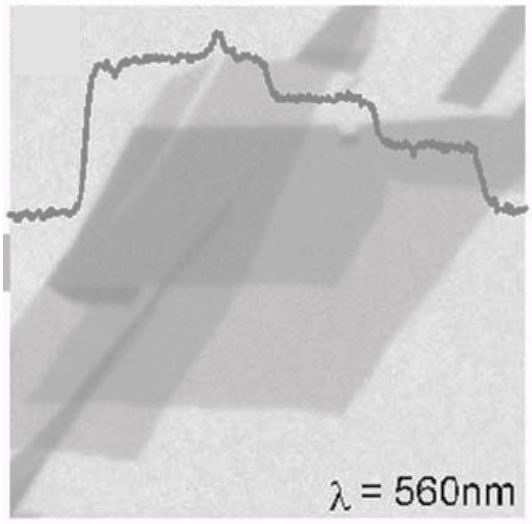

Figure 11: Optical image of a few layer graphene flake with a line intensity profile superimposed, demonstrating the regions covered by one, two, and three layer films. Reprinted with permission from [21]. Copyright 2007, American Institute of Physics.

Atomic Force Microscopy

Atomic force microscopy, also known as AFM, is a high resolution imaging technique in which a several micrometer sized tip on the end of a cantilever is mechanically scanned across a sample. Unlike optical microscopy, it is used to analyze materials on a three-dimensional level, determining specimen thickness on the nanometer scale. While thickness readings do not indicate a change in composition, this instrument can also be operated in a phase imaging mode, which has the ability to resolve the difference between pristine graphene and oxidized graphene due to the variation in interaction forces between the functional groups and the tip [22]. Examples of both height and phase images of graphene oxide and reduced graphene oxide are presented in Figure 12.

The main drawback to this method is its very low throughput. While other types of microscopy can produce an image almost instantaneously, it often takes several minutes to obtain a single AFM reading that is only a few micrometers by a few micrometers in scale. However, it boasts a number of advantages as well, including its unparalleled resolution and

ability to operate in different modes in order to study various other aspects of graphene and its derivatives, such as electrical, magnetic, mechanical, and frictional traits [1]. A discussion on how this instrument is utilized to mechanically characterize graphene films is detailed in the Mechanical Properties portion of Section IV.

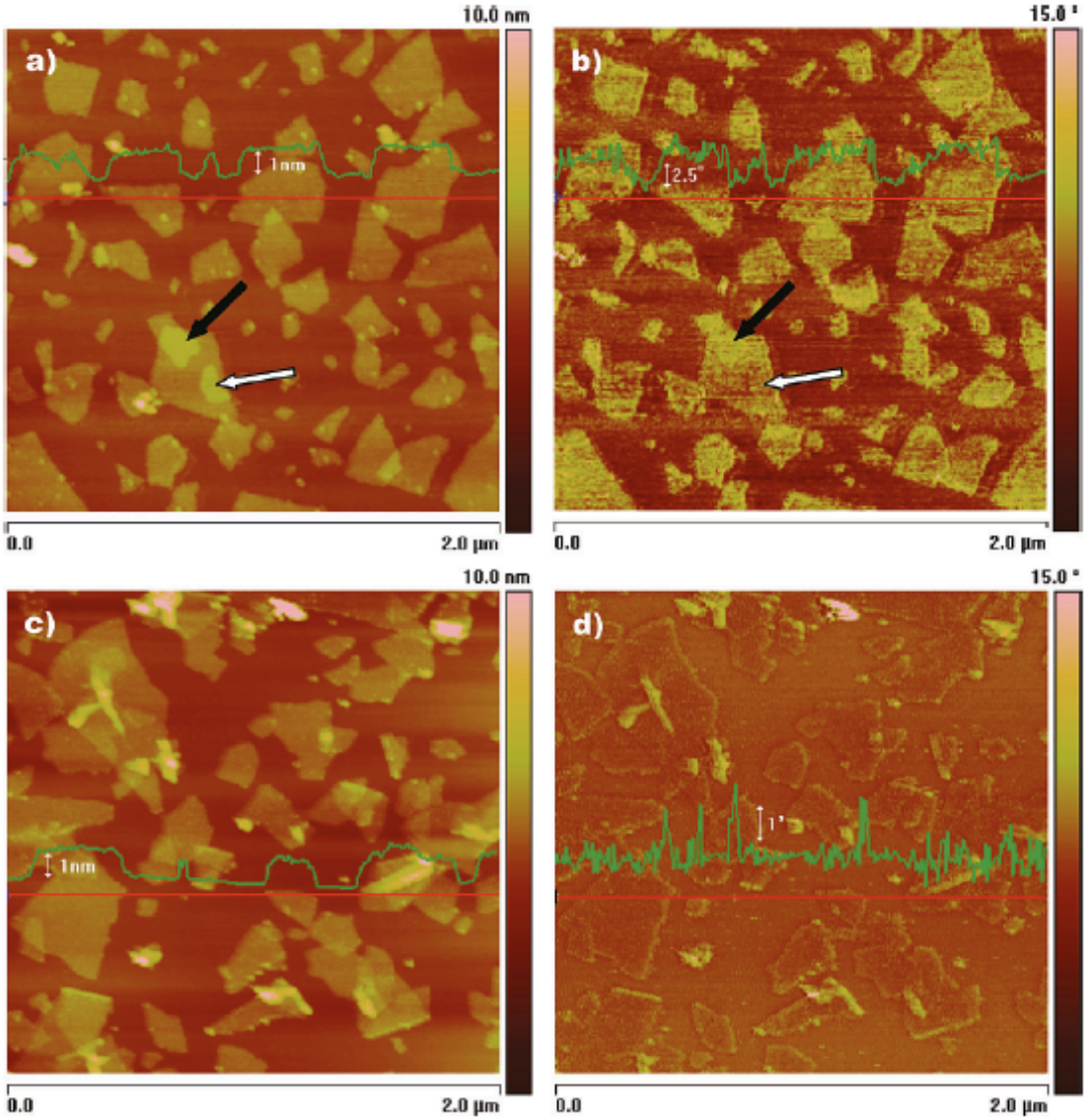

Figure 12: a) AFM image of graphene oxide showing sample thickness with a superimposed line profile. b) Corresponding phase image. c) Thickness image of reduced graphene oxide with a superimposed line profile. d) Corresponding phase image. A significant change in phase is evident upon reduction from graphene oxide to reduced graphene oxide. Reprinted with permission from [22]. Copyright 2009 American Chemical Society.

Electron Microscopy

Three variants of electron microscopy: transmission electron microscopy (TEM), scanning transmission microscopy (STEM), and scanning electron microscopy (SEM), are all employed in the study of graphene. The term "transmission" indicates the transmission of the electron beam through a very thin sample where it is picked up by a imaging detector, and "scanning" indicates the formation of a raster of points on the sample over which the beam is shifted. As its name suggests, STEM utilizes a combination of both of these functions.

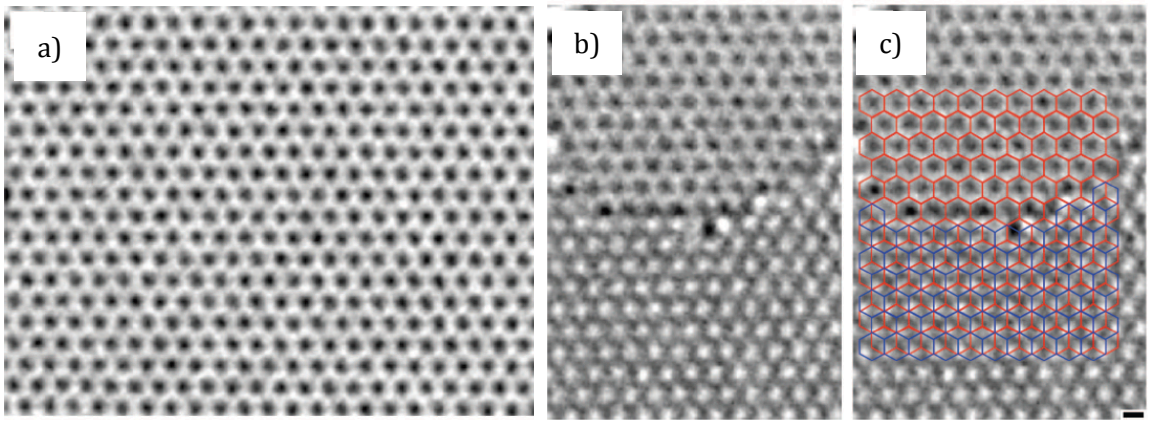

Figure 13: a) HRTEM (high resolution TEM) image of the atomic arrangement of a graphene single layer. Atoms appear white and gaps are black. b) HRTEM image of the transition from monolayer (top) to bilayer (bottom). c) Same image with a superposition of the monolayer structure in red and the bilayer structure in blue. Reprinted with permission from [23]. Copyright 2008 American Chemical Society.

A shortcoming of traditional TEMs is the need to be operated at high voltages in order to achieve resolution high enough to image atomic scale features on samples such as graphene. Such high voltages cause damage and degradation in the delicate sample, rendering it unobservable [1]. However, a new grade of TEM has recently been developed that overcomes this obstacle. Through a combination of aberration correction and a monochromated beam, these instruments can run at operating voltages as low as 80 keV while being able to achieve sub-Ångstrom resolution, enough to image individual atoms in

monolayer and bilayer graphene [23], as seen in Figure 13. The traditional "ball and stick" model is distinct in these images, with carbon atoms appearing bright and gaps in the hexagonal lattice appearing dark [24].

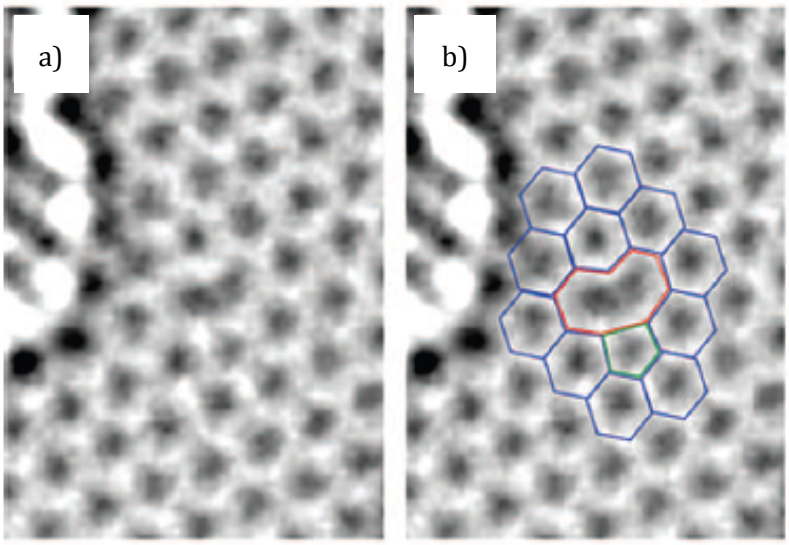

Figure 14: a) HRTEM image of a vacancy in a graphene monolayer. b) Same image with a superposition of atomic structure showing the irregularities in red and green. Reprinted with permission from [24]. Copyright 2008 American Chemical Society.

Defects on the atomic scale have also been imaged using this technique [24], such as the vacancy observed in Figure 14. These instruments have been employed to verify that defects and topological irregularities are linked to a decline in the material's electronic and mechanical performance, as expected [1]. As briefly stated in the Chemically Derived Graphene segment of Section II, TEM studies of GO and rGO have been performed as well. Figures 7 and 8 portray HRTEM images of the atomic structures of GO and rGO, respectively, and demonstrate that the composition consists of pristine graphene areas surrounded by oxygen functional groups. A study of a single layer of reduced graphene oxide with several different structural elements and defects indicated in color is displayed in Figure 15.

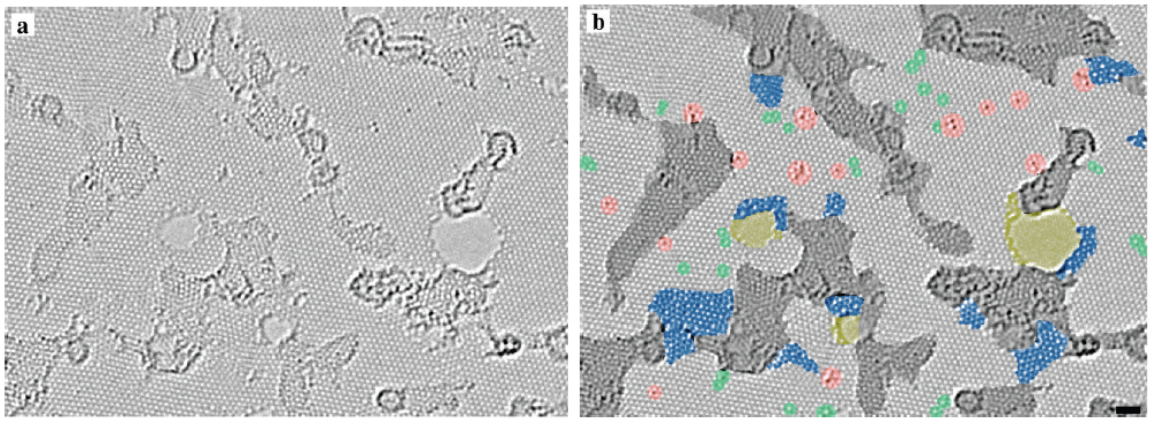

Figure 15: a) HRTEM image of an rGO monolayer demonstrating several defects and topological irregularities. b) Same image with various features highlighted in color. The defect free crystalline graphene area is displayed in the original light gray color. Contaminated regions are shaded in dark gray. Blue regions are the disordered single-layer carbon networks, or extended topological defects, identified as remnants of the oxidation-reduction process. Red areas highlight individual ad-atoms or substitutions. Green areas indicate isolated topological defects, that is, single bond rotations or dislocation cores. Holes and their edge reconstructions are colored in yellow. Scale bar 1 nm. Reprinted with permission from [25]. Copyright 2010 American Chemical Society.

In addition to TEM, STEM has also played an important role in the analysis of the atomic structure of graphene and its derivatives. An example of a high resolution STEM image can be found in Figure 16a. The high angle annular dark field (HAADF) imaging mode of STEM has been proven to be particularly useful, showing atomic lattice, defects, and contaminant atoms as pictured in Figure 16b. Atoms other than carbon are distinguished via atomic number contrast, with heavier elements appearing brighter than the carbon lattice. Graphene thin films have also found an application in electron microscopy as support membranes for TEM grids. The material is thin and transparent enough to provide support for lighter atoms, and its high degree of crystallinity and superior conductivity help to alleviate both background noise and sample charging [1].

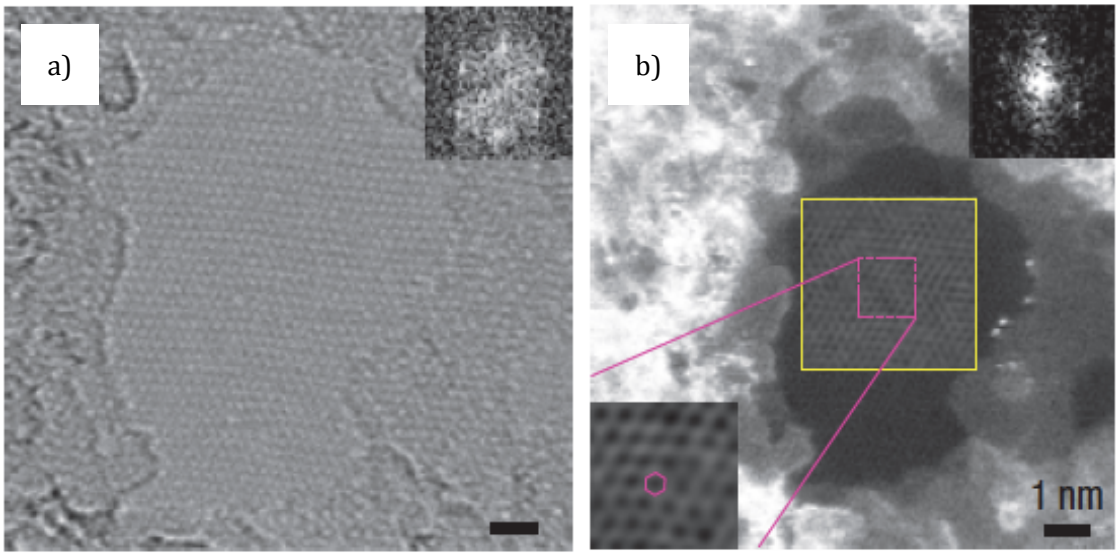

Figure 16: a) High resolution STEM image of a graphene film. b) HAADF image of the same sample with brighter regions signifying heavier elements and a six-sided carbon ring highlighted in purple. Reprinted by permission from Macmillan Publishers Ltd: Nature Nanotechnology [26], copyright 2008.

Raman Spectroscopy

As one of the most informative spectroscopic methods to date, Raman spectroscopy is essential to graphene research. This non-destructive form of analysis is used to evaluate the vibrational, rotational, and other low frequency modes of a given material through the inelastic scattering of light. Because of differences in molecular structure, each individual material emits its own unique Raman "fingerprint". Carbon allotropes exhibit universal Raman shifts at around 1350 cm^{-1}, 1580 cm^{-1}, and 2700 cm^{-1}, known as the G, D, and 2D peaks, respectively. It's the intensity, width, and number of these peaks that allow specific classification. Other information such as the number of layers in a sample, effect of strain, doping concentration, effect of temperature, and presence of defects can also be analyzed from Raman data [1].

In graphitic materials, the G band arises from the doubly degenerate E_{2g} phonon mode at the Brillouin zone center [27]. The D band is due to disorder on the atomic level,

which includes edge effects, ripples, functional groups, and charge puddles [16, 27]. The 2D band is a result of second order zone boundary phonons and occurs at approximately twice the value of shift of the D band [27]. Figures 17 and 18a display all three of these distinctive peaks in the Raman spectra of mechanically exfoliated graphene, graphene oxide, reduced graphene oxide, and bulk graphite.

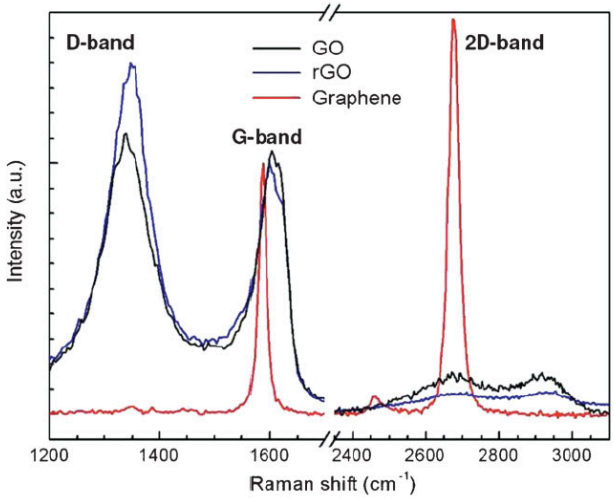

Figure 17: Raman spectra of monolayers of mechanically exfoliated graphene, graphene oxide, and reduced graphene oxide with the G bands normalized. Reprinted by permission from John Wiley & Sons, Inc.: Advanced Materials [16], copyright 2010.

Upon comparison of these four materials, it is evident that both graphene and bulk graphite have sharp, narrow G bands and completely lack the D band present in graphene oxide and reduced graphene oxide, which is attributed to their oxygen functional groups. On the contrary, the 2D band in oxidized graphene is significantly reduced in intensity and shows a much wider, double peak. The elimination of oxygen functional groups during reduction from graphene oxide to reduced graphene oxide is apparent due to the decrease of intensity in the D and 2D bands [16]. Upon examination of the non-oxidized forms, bulk graphite demonstrates a much more intense G peak than graphene, and its 2D band displays both a different shape and intensity [27].

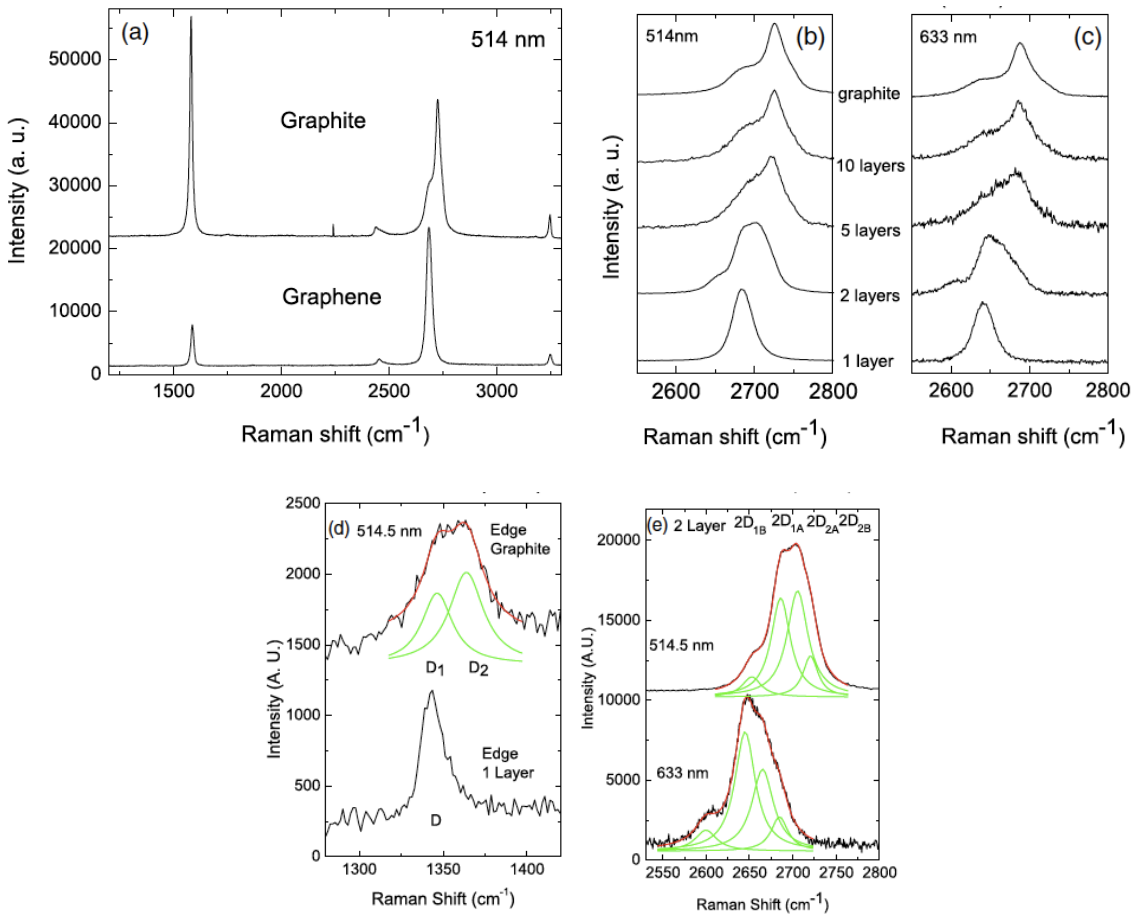

Figure 18: a) Raman spectra of bulk graphite and graphene. b) and c) Sequence of 2D peaks from a graphene single layer up to bulk graphite using a 514 nm and 633 nm wavelength laser, respectively, showing the alteration with varying numbers of layers. d) 2D peaks from monolayer and bilayer graphene, demonstrating the deconvolution of the bilayer peak into two components. e) Deconvolution of bulk graphite's 2D peak into four components. Reprinted with permission from [27]. Copyright 2006 by the American Physical Society.

Another important area of study is the change in Raman data with varying numbers of graphene layers. A. C. Ferrari et al investigated this effect in non-oxidized graphene and determined that the 2D band splits into two components for bulk graphite and into four components for bilayer graphene, as depicted in Figure 18d and 18e. The authors also found that an increase in layers causes a blue shift in the 2D peak, while widening and reducing of the intensity reading [27]. This progression, from monolayer graphene up to bulk graphite, is nicely shown in Figures 18b and 18c.

Fluorescence Quenching Microscopy

Fluorescence quenching microscopy, or FQM, has recently risen to attention as a method to image graphene, graphene oxide, and reduced graphene oxide for quick assessment and manipulation, particularly for the fine-tuning of synthesis processes. The technique involves coating a graphene-based sample with a green fluorescein sodium salt dye and successive imaging with a fluorescence microscope. Visible contrast between the sample and the substrate is a result of the graphitic material's quenching effect on the dye's emission. After analysis, the dye can be rinsed off without disrupting the structure of the sample [28]. A visual sequence of sample observations during this procedure is presented in Figure 19.

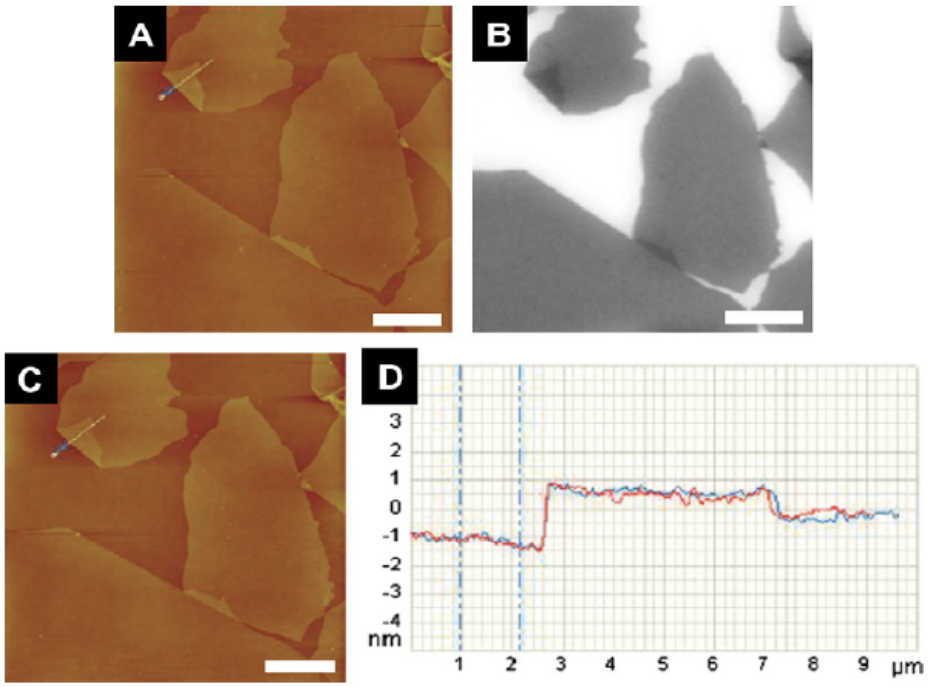

Figure 19: a) AFM image of graphene oxide monolayers before application of the green fluorescein dye. b) Subsequent FQM image of the same area. c) AFM image after cleansing of the dye. d) Before and after line profile readings indicating no substantial change in material thickness due to implementation of the dye. Reprinted with permission from [28]. Copyright 2010 American Chemical Society.

Advantages of FQM include its low cost, time efficiency, and ability to be substrate independent, which is one of the main drawbacks of optical microscopy. However, this method does limit the size of observable samples to microns because of its diffraction limited lateral resolution, and it also prohibits further experimentation with the same sample due to the addition of undesired functional groups to the sample surface from the dye [1].

Part I, Section IV – Properties

Structure

As described in Section I, graphene is a two-dimensional plane of carbon atoms arranged in a hexagonal lattice. Each carbon atom is sp^2 hybridized, with its sp^2 orbitals engaged in σ bonds with its three nearest neighbor atoms and its $2p_z$ orbital contributing to a delocalized network of π bonds [12, 29]. While the σ bonds are energetically stable and do not contribute to electron transport, the vastly interconnected π bond system is key to the material's impressive conductivity. In real space, the graphene unit cell consists of two atoms, A and B, which define two triangular sub-lattices [29], as depicted in Figure 20a. This translates into a subsequent honeycomb lattice in reciprocal space, with a hexagonal first Brillouin zone [3, 12, 29], also pictured in Figure 20a. Another structural quality of graphene is intrinsic corrugations, or ripples [12, 30]. This attribute has been studied via STM and modeled by Monte Carlo simulations, as presented in Figure 20b. While small ripples (heights of <0.5 nm) showed trivial effects on local electrical properties, larger features (heights of 2-3 nm) provided evidence for strain-induced modulations [12].

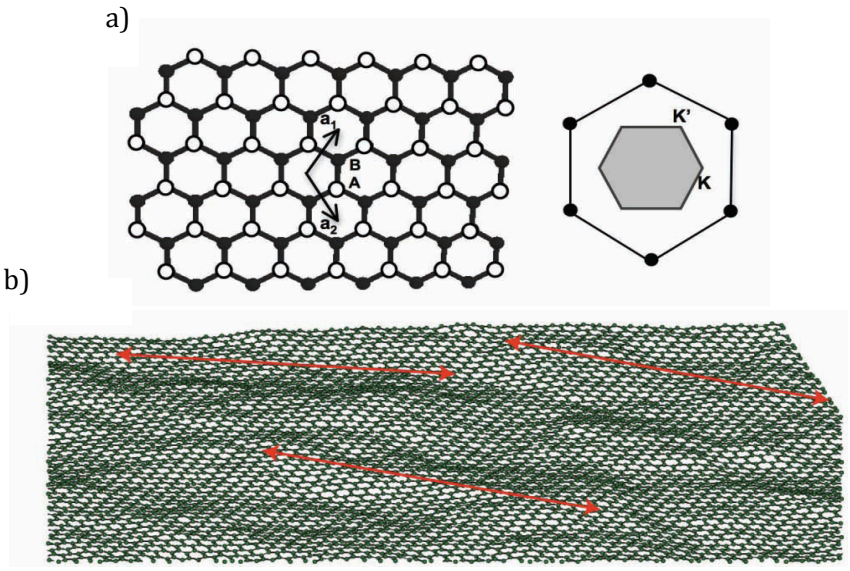

Figure 20: a) Graphene's crystal structure with sub-lattices A and B designated and subsequent first Brillouin zone. b) Monte Carlo simulation of intrinsic corrugations in a graphene film. The red

arrows represent the lateral width of the ripples and are ~80 Å in length. a) Reprinted by permission from John Wiley & Sons, Inc.: Advanced Materials [12], copyright 2007. b) Reprinted by permission from MacMillan Publishers Ltd: Nature Materials [30], copyright 2007.

Electronic Properties

Graphene's extraordinary electronic properties are a direct consequence of its high crystal quality and unique electronic band structure. The high degree of structural symmetry gives rise to two inequivalent points, K and K', which are present along the edge of the first Brillouin zone [3, 12], as indicated in Figure 20a. A crossover of the valence and conduction bands at the Fermi energy occurs at these two points and linear energy dispersion is exhibited within 1 eV of these intersections, resulting in a conical band structure [2, 3, 12] as shown in the inset of Figure 21a. Because of this unique conical configuration, charge carriers within the material behave relativistically and are better described by the (2+1)-dimensional Dirac equation as opposed to the much more conventional Schrödinger equation [2, 3]. Thus, charge carriers are classified as 'massless Dirac fermions' [2, 3, 12] and can be considered electrons without a rest mass, m_0, or neutrinos with the charge of an electron, e [2]. Similarly, K and K' are deemed 'Dirac points' [3, 12].

The overlap of the valence and conduction bands at the Dirac points render graphene a zero band gap semiconductor [2, 12]. This gives rise to an ambipolar electric field effect, or the ability to tune charge carriers between electrons and holes continuously by externally altering the gate voltage. Evidence of this effect is presented in Figure 21a. Carrier concentrations and mobilities have been experimentally determined to be independent of temperature and have values as high as 10^{13} cm^{-2} and 15,000 $cm^2V^{-1}s^{-1}$, respectively, under ambient conditions [2, 3, 12]. After the reduction of impurities and subsequent scattering due to impurities, mobilities of up to 200,000 $cm^2V^{-1}s^{-1}$ have been

achieved, a phenomenal quantity for room temperature [12]. The result of these two substantial attributes is ballistic transport (conductivity without scattering) on submicrometer scales [2, 3, 12]. Analysis of graphene's conductivity and Hall coefficient revealed that both were found to be a function of gate voltage [31], as displayed in Figures 22a and 22b, respectively. The expected ambipolar effect is present in the change in Hall coefficient with respect to gate voltage. Conductivity measurements, however, showed a peculiar trend: the existence of a minimum value at the limit of no charge carriers [3]. While all other known materials ultimately experience a metal-to-insulator transition at the zero field limit, graphene consistently shows a minimum conductivity of $(4e^2)/h$ [2, 3].

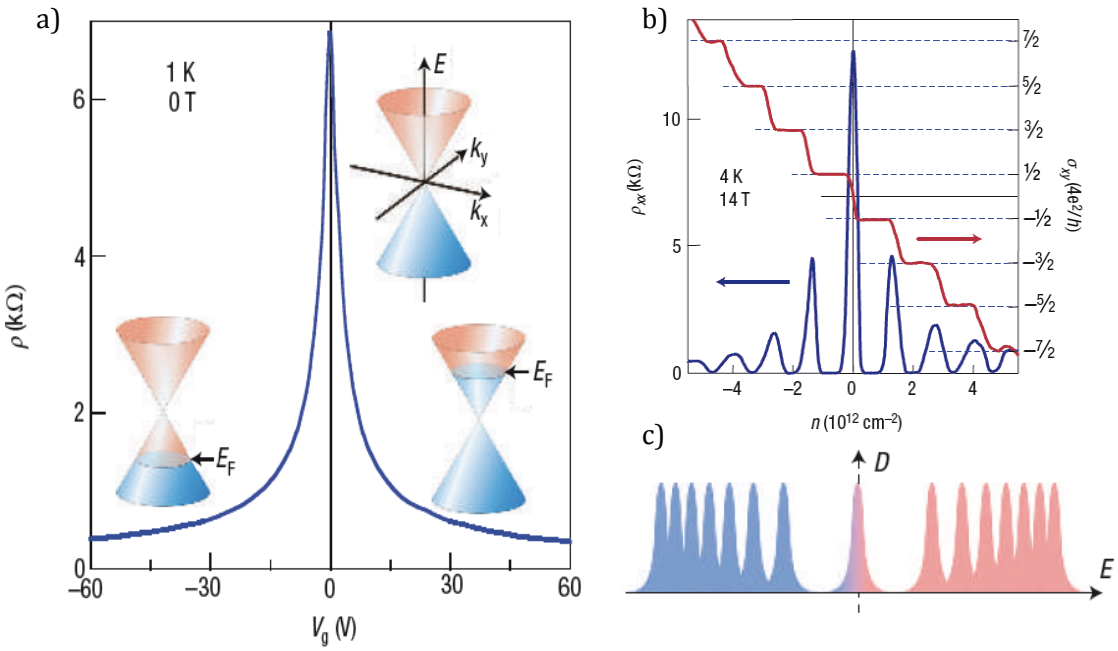

Figure 21: a) Plot of resistivity (ρ) vs. gate voltage (V_g) in monolayer graphene demonstrating the ambipolar effect. Insets show the conical band structure and resultant changes in Fermi energy (E_F) with variation of V_g. b) "Half-integer" quantum Hall effect present in a graph of Hall conductivity (σ_{xy}) vs. carrier concentration (n). c) Depiction of Landau levels in density of states (D) vs. energy (E). The relationship follows the equation $E_N \propto \sqrt{N}$, where N is the number of Landau levels. Reprinted by permission from MacMillan Publishers Ltd: Nature Materials [2], copyright 2007.

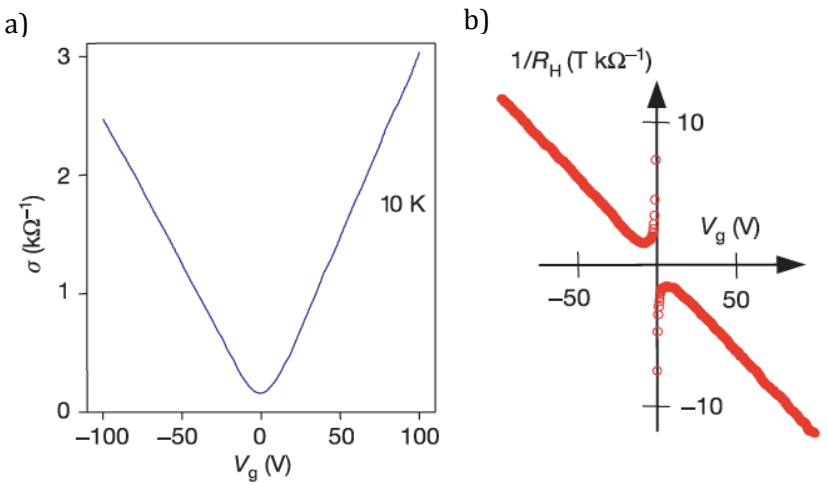

Figure 22: a) Relationship between conductivity (σ) and gate voltage (V_g) indicating a minimum value of conductivity at $V_g = 0$. b) Evidence of the ambipolar effect in a plot of inverse Hall coefficient ($1/R_H$) as a function of gate voltage (V_g). Reprinted by permission from MacMillan Publishers Ltd: Nature Materials [31], copyright 2005.

Another significant electronic feature in single layer graphene is the existence of an anomalous "half-integer" quantum Hall effect at low and room temperatures [2, 3, 12]. This arises from the presence of a quantized Landau level at zero energy, which is comprised of both electrons and holes [2]. The trend is evident in measurements of Hall conductivity vs. carrier concentration [2, 3, 12], as pictured in Figure 22b, where plateaus in Hall conductivity are present at half-integer multiples of $4e^2/h$ [3, 12]. Other phenomena unique to graphene include suppression of weak localization, Klein tunneling (the transmission of charge carriers through high and wide potential barriers), quasi-particle pseudospin (an indication of sublattice A or B), and chirality (a projection of pseudospin on the direction of particle motion) [2, 3].

Optical Properties

Graphene's exceptional optical image contrast allows single layers of the material to be visible on substrates such as SiO_2/Si and Si_3N_4/Si, as described in the Optical Microscopy

segment of Section III. This phenomenon arises from interference between the material and the substrate, where the dielectric acts as a spacer [1, 32]. Contrast is defined by the following equation: $C = (R_{graphene} - R_{dielectric})/(R_{graphene} + R_{dielectric})$, where $R_{graphene}$ is the reflected intensity from the material and $R_{dielectric}$ is the reflected intensity from the bare substrate. If $C = 0$, the material will not be detectable, if $0 < C < 1$, the material will be brighter than the substrate, and if $0 > C > -1$, the material will be darker than the substrate [1]. Contrast varies with the number of layers and can be amplified by adjusting the spacer thickness or the light wavelength and incident angle [1, 12, 32]. The monolayer refractive index has been found to be $n = 2.6 - 1.3i$ within the visible spectrum [12].

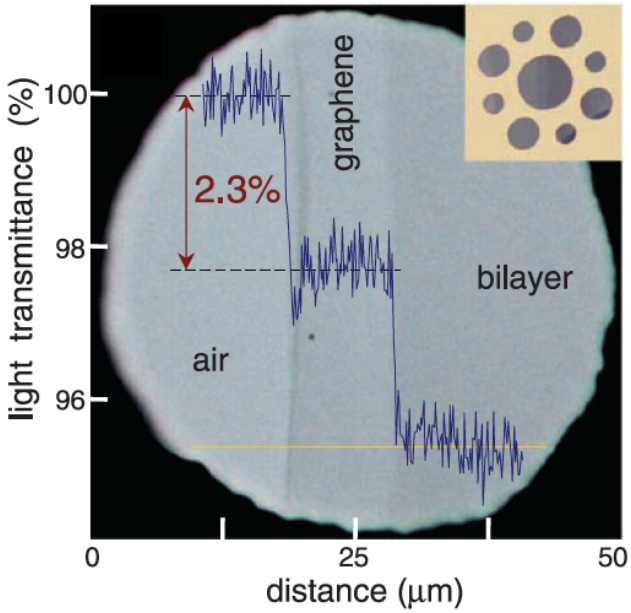

Figure 23: Image of a 50 μm aperture partly masked by single and bilayer graphene films with a measurement of optical transmittance of white light vs. distance superimposed, demonstrating the proportional effect of an additional graphene layer. Inset shows the experiment design. From [33]. Reprinted with permission from AAAS.

Graphene also exhibits a high optical transmittance of white light, which can be represented by the following equation: $T = (1 + 0.5\pi\alpha)^{-2} \approx 1 - \pi\alpha$, where $\alpha = 1/137$, the fine structure constant. Thus, transmittance is established to be 97.7% and absorption,

represented by $A \approx (1 - T) \approx \pi\alpha$, is consequentially 2.3%. Both of these properties are directly proportional to the number of layers, with each layer absorbing 2.3% of incident light [33], as portrayed in Figure 23. Another uncommon optical attribute of graphene is the existence of saturable absorption [12, 32]. This occurs when the intensity of incident light reaches a certain value, an effective saturation point, at which Pauli blocking starts to interfere with the amount of photon absorption per layer. Because pristine graphene is a zero band gap semiconductor, it is not expected to exhibit photoluminescence. However, both chemical and physical treatments to lessen the connectivity of the π bond network have been shown to induce this effect. Graphene oxide demonstrates photoluminescence over a broad scale, and individual graphene flakes subjected to a mild oxygen plasma treatment can also be made luminescent. Untreated graphene layers have been revealed to emit broadband nonlinear photoluminescence upon non-equilibrium optical excitement, which is alleged to be due to recombination of hot electrons and holes [32].

Mechanical Properties

In addition to its noteworthy electronic and optical properties, graphene also boasts astonishing mechanical traits. Not only is it the strongest material ever known, with a tensile strength of 42 Nm^{-1} and a fracture strength of 130 GPa, it is also the stiffest material on record with a Young's modulus of ~1 TPa [3, 34]. These mechanical properties are attained through nanoindentation with an atomic force microscope, a method in which an AFM tip is applied to a monolayer film stretched over an opening in the substrate [34], as depicted in Figure 24. Graphene has also been discovered to show incredible mechanical flexibility. Upon deposition on a silicone substrate, single layer films can be elastically extended up to 6%, with a failure strain of 12%. Stretching on a pre-strained silicone substrate displays even higher values of up to 25%. Electrical resistance has been

discovered to remain stable up to 11%, with an order of magnitude change occurring around 25% [35]. Many other electronic and optical properties have also been shown to maintain their integrity upon stretching [3]. A variety of graphene oxide "papers", consisting of continuous assemblies of individual platelets, have also been produced and studied, demonstrating an average elastic modulus of ~32 GPa and a maximum fracture strength of ~120 MPa [12].

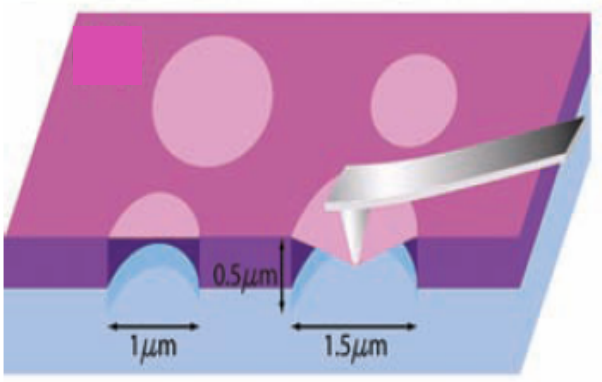

Figure 24: Illustration of the nanoindentation process with an AFM tip on a graphene layer stretched over a circular void. From [34]. Reprinted with permission from AAAS.

Thermal Properties

Because of the low carrier density in non-doped graphene, thermal conductivity is primarily influenced by phonon transport within the material. While simulations have predicted values of ~6000 $Wm^{-1}K^{-1}$, it has been experimentally shown that a monolayer of suspended graphene displays an actual thermal conductivity of around 5300 $Wm^{-1}K^{-1}$, higher than that of diamond [12]. For example, A. A. Balandin et al performed thermal measurements as described in Figure 25 on a piece of mechanically exfoliated graphene. The monolayer was applied over a trench in the substrate and a focused laser beam was used as a heat source. The temperature rise in the thin film produced a red shift in the Raman G peak due to phonon softening, and the subsequent data was analyzed to determine a conductivity of 5000 $Wm^{-1}K^{-1}$ [36]. Other published thermal conductivity values include:

~2500 $Wm^{-1}K^{-1}$ for CVD graphene on a thin silicon nitride film and ~600 $Wm^{-1}K^{-1}$ for mechanically exfoliated graphene on a SiO_2 substrate [12].

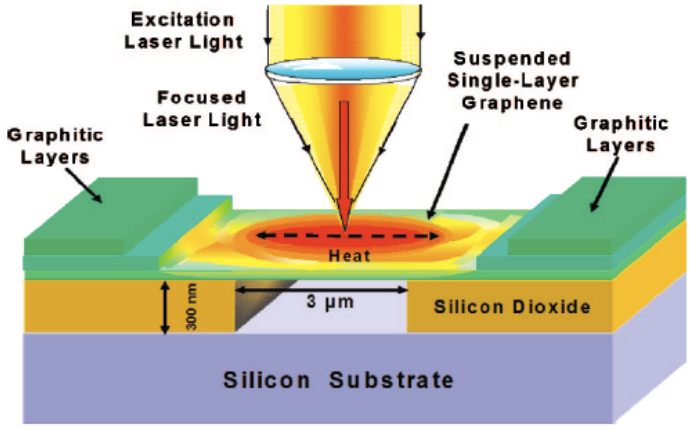

Figure 25: Schematic of a thermal conductivity experiment in which a single layer of graphene in suspended over a channel and subjected to a focused laser. Reprinted with permission from [36]. Copyright 2008 American Chemical Society.

Part I, Section V – Applications

Transparent Conductive Films

Indium tin oxide, or ITO, is currently dominating the market in transparent electrodes but because of its progressive inaccessibility, high cost, and brittle nature, alternative materials are being sought out. Graphene and its derivatives provide a huge advantage over ITO due to its availability and remarkable electronic, optical, mechanical, and structural properties [37]. It is highly conductive, physically flexible, has an optical absorption of 2.3% per layer, is atomically thin, and maintains the integrity of its properties upon mechanical deformation [12, 37]. A graphical comparison of the transmittance of graphene to that of ITO and fluorine doped tin oxide (FTO) can be found in Figure 26.

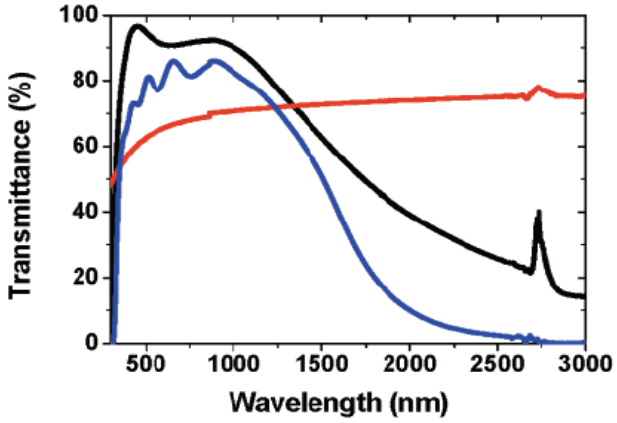

Figure 26: Transmittance comparison of a ~10 nm graphene thin film, ITO, and FTO represented by red, black, and blue curves respectively. Reprinted with permission from [38]. Copyright 2008 American Chemical Society.

Experimental devices have been fabricated with graphene synthesized via reduction of graphene oxide, CVD on Ni and Cu substrates, liquid-liquid assembly, spin coating, and spray deposition, just to name a few [12, 37]. These devices showed sheet resistance values ranging from 100 Ω/□ all the way up to 2×10^7 Ω/□ and transmittance from 70% to 96%. For comparison, the resistance of pristine graphene is 30 Ω/□ [12]. An example of one of these experimental devices is a dye-sensitized solar cell created by Wang et al as seen in

Figure 27. It utilizes electrodes composed of thermally reduced GO films and demonstrated a transparency of 70% in the 1000 to 3000 nm wavelength range and conductivity of 550 S/cm [38]. Mechanically flexible devices have also been developed and studied as well, for example, a graphene film transferred to a polyethylene terephthalate (PET)/polydimethylsiloxane (PDMS) substrate, as pictured in the inset of Figure 28. Resistance was measured as a function of bending radius, displayed in the graphical portion of Figure 28, and doesn't show a significant increase until 2.3 mm (a subsequent tensile strain of 6.5%) and exhibits full recovery even after reaching a radius of 0.8 mm (a tensile strain of 18.7%) [35].

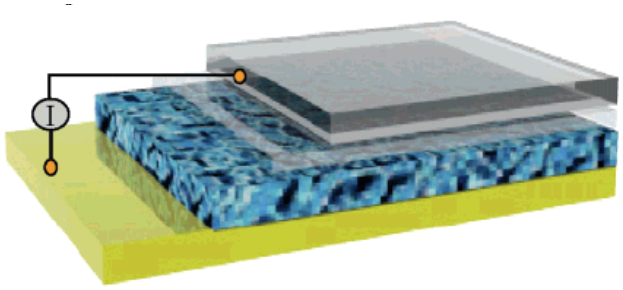

Figure 27: Diagram of a dye-sensitized solar cell employing from top to bottom: rGO as an electrode, compact TiO_2, a dye-sensitized heterojunction, and gold. Reprinted with permission from [38]. Copyright 2008 American Chemical Society.

It's been determined that while solution processed CDG provides the most convenient and scalable production route for transparent conductive films, its sheet resistance varies over a wide range depending on the surface functionalities and defects introduced during processing [12]. On the other hand, synthesis by CVD and subsequent substrate transfer provides high quality, continuous films, but isn't quite applicable to large-area devices at the moment [37]. In conclusion, graphene shows immense potential in the field of transparent conductive films, but more work is needed to both enhance the quality of graphene films and establish a production method applicable for large-scale implementation [12, 37].

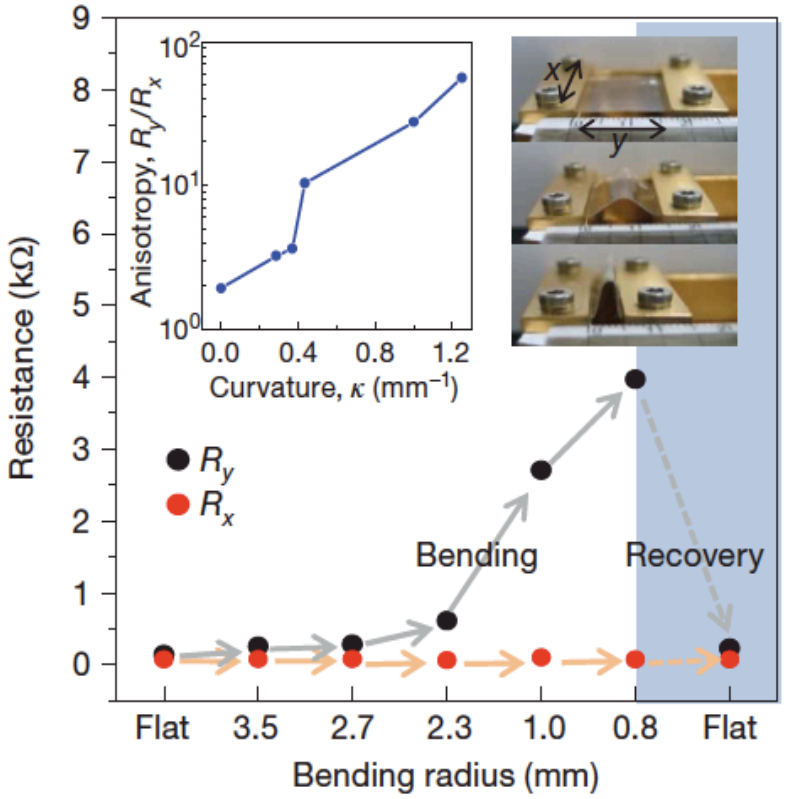

Figure 28: Plot of bending radius vs. resistance of a graphene film on a PET/PDMS substrate. The left inset shows the relationship between curvature and anisotropy and the right inset demonstrates the experimental procedure. Reprinted with permission from Macmillan Publishers Ltd: Nature [35], copyright 2009.

Field Emission Devices

Another potential application of graphene is in field emission (FE) displays. FE is an electron emission effect in which electrons are emitted from a source material via employment of a high electric field. This can be achieved by field enhancement at the tip of a pointed object. In order to form these sharp tips with graphene, the material needs to be oriented in a nonparallel fashion with respect to the substrate. Because most graphene synthesis techniques result in flat layers, the only straightforward production method for this application is PECVD. This technique also allows for direct deposition on metal substrates, eliminating the need for further processing. Vertically aligned cathodes

produced via this method have shown a turn-on electric field measurement of 1 V/μm and a field enhancement factor of ~7500, with a current density of 14 mA/cm^2. A shortcoming to this approach, however, is the limited control of flake density [12].

Other experimental FE devices have been created with rGO/polymer composite thin films and graphene produced via electrophoretic deposition. These alternative materials have been determined to have turn-on field readings from 2.3-4 V/μm and field enhancement factors in the range of 1200-3700, noticeably inferior to those of PECVD graphene [12]. Overall, graphene's impressive properties do make it a valid candidate for FE applications, but much more work is needed before industry implementation.

Sensors

One of the most enticing applications of graphene is in the field of sensors, detecting materials varying from gases to biomolecules. The operational theory behind this function is an alteration of graphene's electricity conductivity upon adsorption of molecules onto the material surface. A charge transfer occurs between the graphene and the adsorbed molecule, with one species acting as a donor and the other as an acceptor, thus changing the thin film's overall electronic properties [12, 37]. Graphene also possesses some unique properties that aid it in being able to sense up to a single atom or molecule. These qualities are as follows: its 2-D nature so that the whole volume is exposed to any incoming molecules, its high conductivity and low Johnson noise allowing a slight change in conductivity to be noticeable, its low degree of crystal defects prohibiting noise from thermal switching, and the ability of four probe measurements to be taken with electrical contacts displaying low resistance [37].

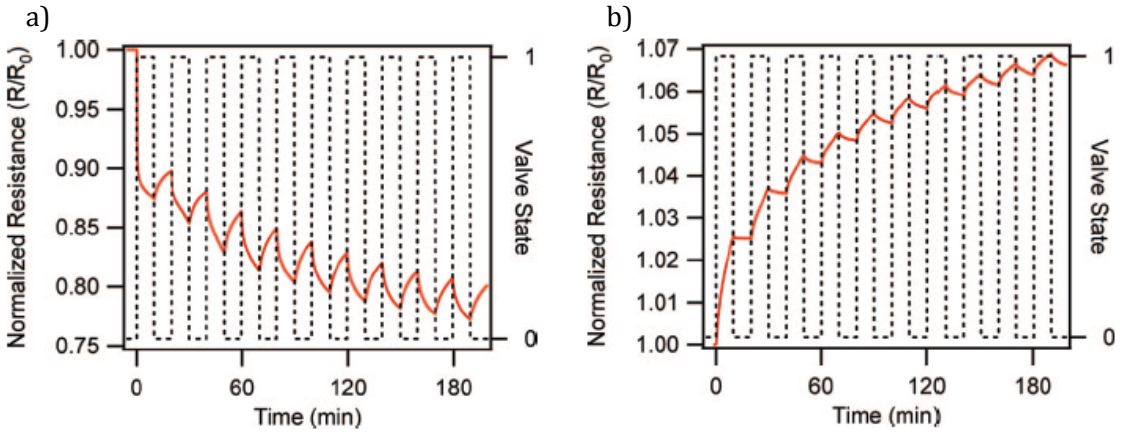

Figure 29: a) NO_2 detection via a graphene thin film. b) NH_3 detection via a graphene thin film. Reprinted with permission from [39]. Copyright 2009 American Chemical Society.

Graphene implemented in sensors can be made through a variety of synthesis methods and are generally applied to silicon or Si/SiO_2 substrates with gold or titanium electrical contacts [37]. These devices have shown particularly good sensing abilities of NO_2, H_2O, NH_3, and CO gases. It is worth nothing that upon interaction with the graphene film, NO_2 and H_2O gases act as acceptors and NH_3 and CO gases act as donors [12]. Fowler et al have demonstrated the detection of NO_2 and NH_3 gases with graphene-based devices [39], as presented in Figure 29. Graphene thin films have been shown to be fully recoverable after sensing via vacuum annealing or UV exposure. Examples of biomaterials that have been recognized by graphene-based sensors include glucose oxidase, catecholamine neurotransmitters (such as serotonin and dopamine), and cadmium ions [37].

Batteries

Li-ion batteries have been a staple in modern technology due to their clean nature and renewability. Anodes in current Li-ion batteries are composed of bulk graphite, because of its reversibility and specific capacity. Due to technology's relentless demand for batteries with higher energy density and durability, alternative materials are consistently

being sought out. Graphene has been proposed to replace graphite as an anode material, because of its superior electronic properties, high surface area, and chemical tolerance [37]. Paek et al have demonstrated a graphene-nanoparticle composite for this very purpose. In their study, the authors synthesized graphene nanosheets coated with SnO_2 nanoparticles, as demonstrated in Figure 30. The composite material exhibits a high degree of lithium storage capacity due to the intercalation of lithium ions into both the nanosheets and the nanoparticles [40]. In reality, very few studies on graphene as an anode in Li-ion batteries have been published, thus plenty of future research is necessary before implementation into a marketable appliance [37].

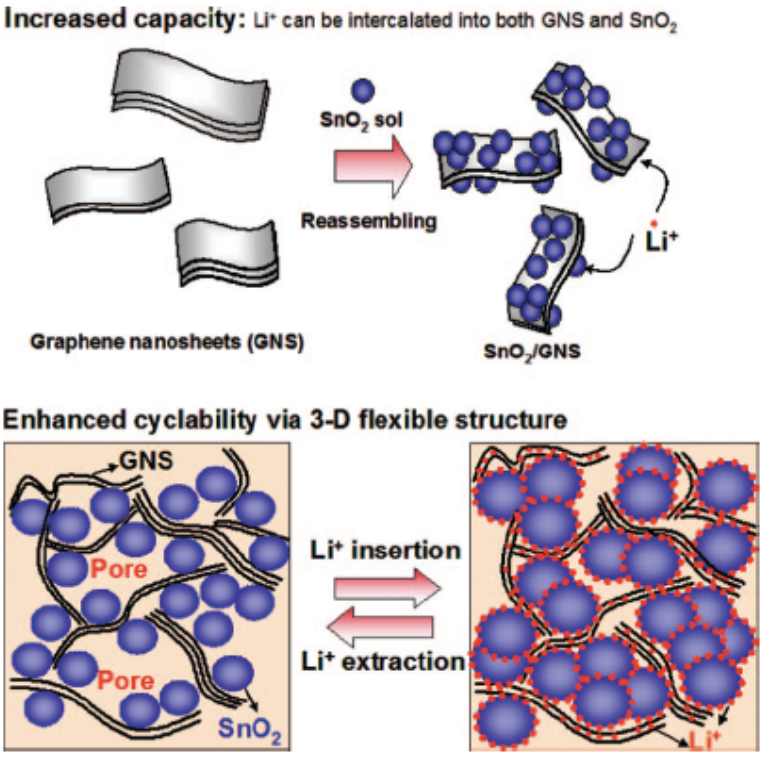

Figure 30: Schematic of the synthesis, structure, and capabilities of SnO_2 nanoparticles on graphene nanosheets. Reprinted with permission from [40]. Copyright 2009 American Chemical Society.

Field Effect Transistors

Field effect transistors, or FETs, have been fabricated with several different forms of graphene, including pristine graphene, bilayer graphene, and graphene nanoribbons (GNRs). Pristine graphene devices are created with a single back gate and show field effect mobilities that are an order of magnitude higher than those fashioned with silicon. CVD on Cu films has been proposed as a method for large-scale production of these types of FETs with identical electronic properties. However, due to the fact that pristine graphene is a zero gap semiconductor, as discussed in the Electronic Properties segment of Section IV, minimal on/off current ratios have been reported for these devices [12]. A solution to this obstacle is inducing a band gap in the material that will allow the current to be fully shut off [12, 37].

Band gap introduction has been achieved in a variety of graphene derivatives: epitaxially grown graphene on SiC substrates, bilayer graphene, and GNRs. Epitaxial graphene on SiC has been shown to possess a band gap of up to 0.26 eV as a result of electronic interaction between the film and the substrate. Upon the addition of a top gate to an FET device and the employment of a perpendicular electric field, bilayer graphene has been demonstrated to have a tunable band gap of up to 0.25 eV in ambient conditions [12].

However, the most prominent approach to creating a band gap in graphene has been the fabrication of GNRs, which confines the boundaries of graphene into a quasi 1-D form displaying narrow widths and atomically smooth edges. A complete overview of synthesis techniques is described in the Graphene Nanoribbon portion of Section II. Lithographic routes have produced GNRs with widths from 20 to 30 nm and chemical synthesis methods have resulted in 10 to 15 nm width GNRs. Studies of GNR FETS have revealed that the energy gap is inversely proportional to the nanoribbon width, with a current maximum band gap of 0.4 eV. An example of experimental devices made with GNRs

can be found in Figure 31. A variety of theoretical studies on GNR FETs have also been published, hypothesizing the properties of these devices with respect to edge roughness, chemical doping, chirality, contacts, and carrier scattering [37]. Just like all new technology, graphene-based FETs are still in the primary stages of their development, therefore more time and research is needed to fully realize their real world potential.

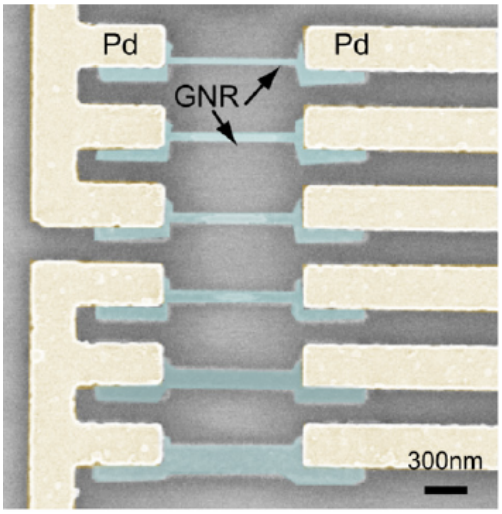

Figure 31: SEM image of FET devices fabricated with GNRs varying in width from 20 nm to 200 nm. Reprinted from [41] with permission from Elsevier.

Part I, Section VI – Summary/Future Potential

In this article, the history, synthesis, characterization, properties, and applications of graphene and its derivatives have been reviewed. Instigated by K. S. Novoselov and A. K. Geim's groundbreaking discovery of freestanding 2-D atomic layers in 2004, research in the field of graphene has grown exponentially over the last decade. Synthesis techniques include mechanical exfoliation (physically and in solution), CVD on both high and low carbon solubility metal substrates and PECVD, thermal decomposition of SiC and epitaxial growth on various metal substrates, and oxidation and exfoliation of bulk graphite into GO followed by thermal or chemical reduction to rGO, all of which demonstrate both advantages and disadvantages. Once fabricated and/or isolated, graphene thin films are characterized by optical microscopy, AFM, electron microscopy (SEM, TEM, and STEM), Raman spectroscopy, and FQM, among others.

Numerous studies of graphene have shed light on its phenomenal structural, electronic, optical, mechanical, and thermal properties. Structurally, graphene is an atomically thin material composed of a hexagonal lattice of carbon atoms. Electronically, it demonstrates a zero band gap semiconducting quality, an ambipolar effect, a finite zero field minimum conductivity, and a "half-integer" Quantum Hall effect. Optically, it displays an absorption quantity of 2.3% per layer, saturable absorption, and the ability to be visualized on certain substrates due to contrast arising from interference between the film and the substrate. Mechanically, it boasts a tensile strength of 42 Nm^{-1}, a fracture strength of 130 GPa, a Young's modulus of ~1 TPa, incredible flexibility with an elastic extension of up to 6% and a failure strain of 12%, and conservation of its electronic and optical integrity upon stretching up to 25%. Thermally, it exhibits a conductivity of around 5300 $Wm^{-1}K^{-1}$. Collectively, these qualities have justified its implementation in transparent conductive films, FE devices, sensors for gas and biomolecules, anodes in Li-ion batteries, and FETs.

Despite all of these remarkable discoveries, perhaps the most exciting aspect of graphene is the fact that it's only in the beginning stages of development. So much more research and experimentation is required before its true potential can fully be realized. Some areas in need of advancement are: large-scale production of high electronic quality material, methods of growth directly on a wide variety of substrates, and better ways to control the width, thickness, and continuity of the films during fabrication. Upon the elimination of these boundaries however, graphene and its derivatives show immense potential to replace such conventional materials as silicon in transistors and ITO in transparent displays, and ultimately possess a very real capability to revolutionize the field of nanotechnology and electronic devices.

Part II – Graphene Growth on Insulating Substrates via Nickel Diffusion

Part II, Section I – Introduction/Background

As extensively covered in the previous review, graphene and its derivatives exhibit extraordinary structural, electronic, optical, mechanical, and thermal properties, which justify its capacity to transform the technology behind electronic devices. Perhaps one of the applications closest to realization is the implementation of graphene as a transparent, flexible, conductive film for optical displays. The main issue opposing this achievement is the feasibility to manufacture large-area, high electronic quality sheets of the material on an industrial level. Another obstacle is developing a reliable synthesis method that is substrate independent, eliminating the hassle of transferring the film from growth substrate to device substrate.

Of the current prominent synthesis techniques available, each exhibit advantages and disadvantages. Mechanical exfoliation results in pristine graphene films with a very high degree of crystallinity and continuity, but due to the nature of the process can only be produced on a very small scale and are more appropriate for research purposes. On the other hand, CDG sheets created by oxidation and successive reduction of graphite are much more manageable and can easily be manufactured on an industrial scale, but lack the remarkable qualities of pristine graphene. Lastly, thin films fabricated by CVD of hydrocarbon gases onto metal substrates also exhibit potential to be scaled up for industrial purposes, however the high temperature (~1000°C) growth process is restricted to conducting substrates and thus a subsequent transfer onto the desired substrate is necessary. This thesis proposes an alternate synthesis method to prepare pristine graphene on insulating substrates in a lower temperature (50° – 400°C) environment, while utilizing the concept behind CVD fabrication on a high carbon solubility metal.

The chief objective of this procedure is to employ the diffusion of carbon into nickel to grow graphene layers. Unlike CVD, where carbon from a hydrocarbon gas is diffused into a solely nickel or copper foil then allowed to precipitate out to form graphene, this work investigates the diffusion of carbon through a thin nickel layer directly onto an insulating substrate. The experimental set-up entails the evaporation of a layer of nickel on top of a SiO_2/Si substrate, which is then coated with a carbon source and annealed to initiate the diffusion of carbon into the metal. Once the carbon fully traverses through the layer, it should precipitate out at the interface between the nickel and the SiO_2/Si substrate, forming a graphene thin film.

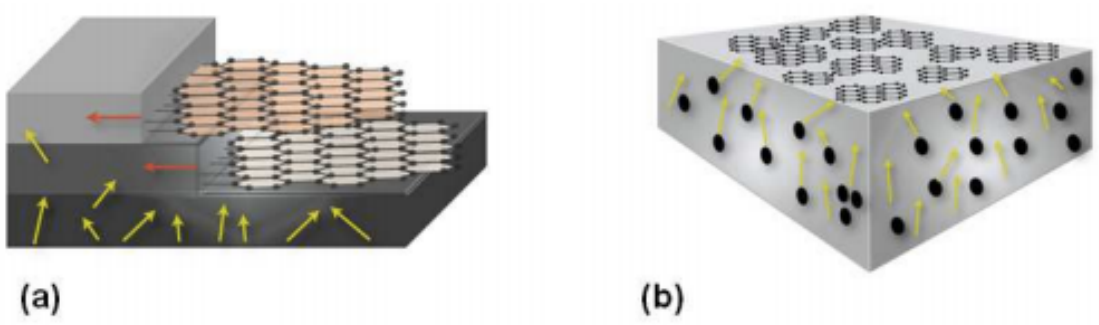

Figure 32: Mechanisms of growth for carbon diffused in nickel. a) High quality graphene layers whose growth initiates at Ni grain boundaries and propagates laterally. b) Surface precipitation of carbon into randomly aligned "nanocrystalline" films. Reprinted by permission from [42].

The reason behind the selection of nickel as the diffusion layer is the very high solubility and diffusivity of carbon in nickel. Carbon atoms diffuse into the metal with a relatively low activation energy of 1.74 eV [43]. This combined with an elevated temperature due to annealing results in fairly quick integration of the two materials. It has been hypothesized that the migration of carbon atoms out of the metal during quenching takes place via two different mechanisms [42], as illustrated in Figure 32.

The first route, pictured in Figure 32a, entails the growth of continuous graphene layers from the intersection of the surface and the nickel grain boundaries. This occurs

when carbon atoms migrate to the grain boundaries and begin to precipitate on the surface. As more carbon diffuses towards these boundaries and out of the metal, graphene layers start to generate and propagate laterally outward from these nucleation sites. On the contrary, the second route, presented in Figure 32b, involves the growth of randomly oriented, "nanocrystalline" graphene films from arbitrary nucleation sites across the nickel surface. It is suggested that this occurs in the event of high supersaturation of carbon within the metal. Unlike the first mechanism in which the carbon migrates over long distances to the grain boundaries, this process indicates only local transport of the carbon atoms to their random growth points [42].

Overall, this work aims to establish a novel procedure for the synthesis of scalable, high quality graphene thin films via diffusion through nickel onto insulating substrates that can be implemented on an industrial level.

Part II, Section II – Experimental Procedure

A 40 nm layer of nickel was deposited via thermal evaporation furnace onto oxidized silicon substrates topped with an oxide layer of 300 nm with dimensions of approximately 1 cm by 1 cm. Carbon solution was fabricated by diluting graphite powder in isopropyl alcohol and centrifuging twice at 3000 rpm for 30 minutes each to remove large aggregates. This solution was then spin coated on top of the $Ni/SiO_2/Si$ substrates, as depicted in Figure 33. Spin coating conditions were as follows: 100 rpm for 2 seconds, 500 rpm for 5 seconds, and 3000 rpm for 60 seconds. After preparation, the samples were annealed in a tube furnace under a 93% nitrogen/7% hydrogen environment at 50°C, 100°C, 150°C, 200°C, or 400°C for 4 hours to generate the carbon diffusion. They were then allowed to cool and etched in a 5:1 hydrochloric and nitric acid solution overnight to remove the nickel and excess carbon solution.

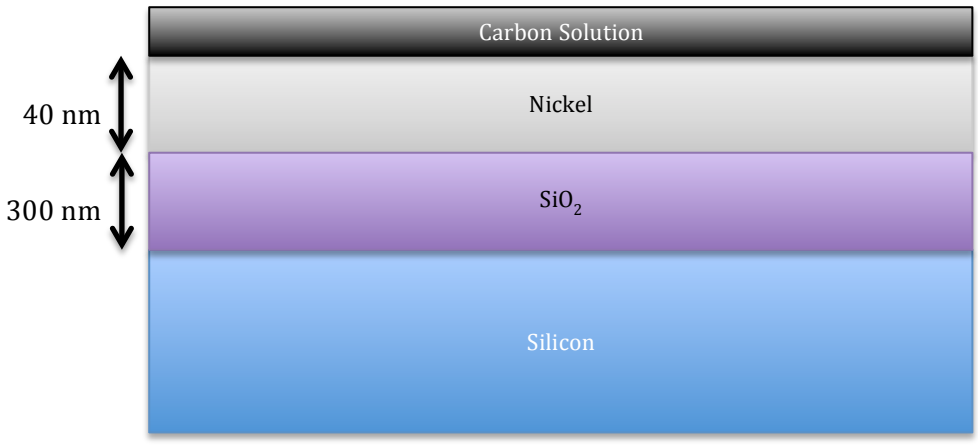

Figure 33: Schematic of the silicon substrate, 300 nm SiO_2 layer, 40 nm nickel layer, and spin coated carbon solution, from bottom to top.

Part II, Section III – Results/Discussion

The prepared samples were analyzed using Raman spectroscopy to identify the types of graphitic materials present. Measurements were performed on a Renishaw spectrometer with the 50x objective and 514 nm wavelength laser selected and were obtained at 10% laser power in 3 acquisitions of 10 seconds each. Raman spectra and their corresponding optical images were taken at various locations and thicknesses along the surface, averaging 5 readings per sample. An example of a Raman spectrum and optical image from a specimen that had been annealed at 200°C can be found in Figure 34.

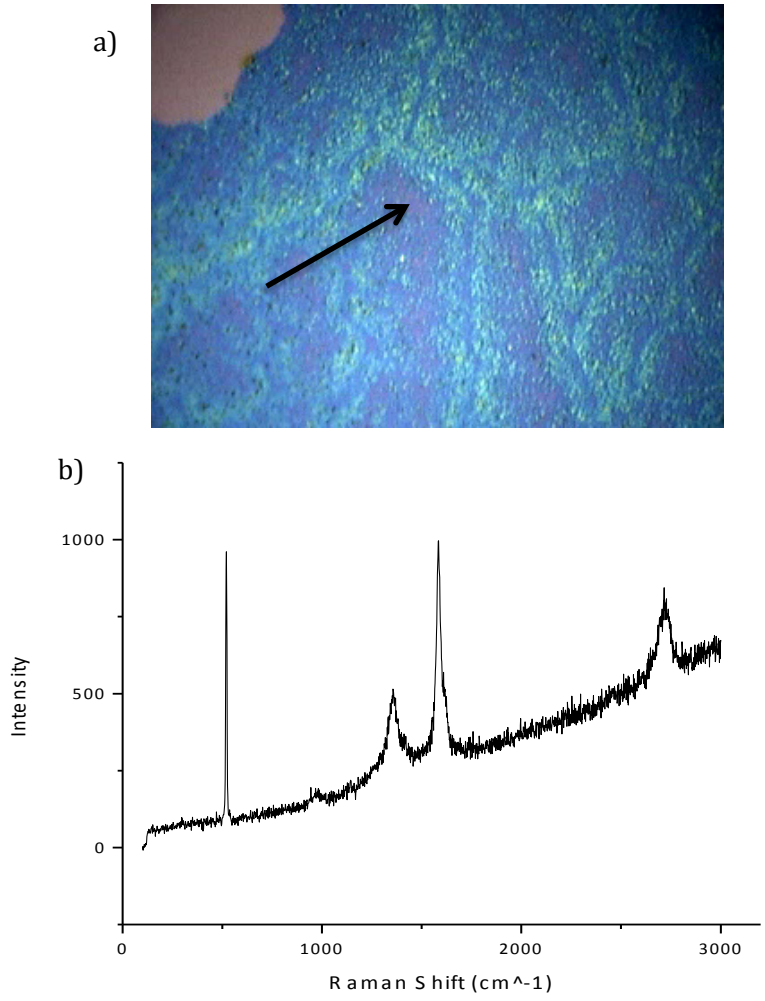

Figure 34: a) Optical image of the surface of the specimen annealed at 200°C with the graphitic film appearing green, blue, or purple depending on its thickness and the bare SiO_2/Si substrate present in

the upper left corner. The tip of the arrow indicates where the Raman measurement was taken. b) Corresponding Raman spectrum showing clear D, G, and 2D peaks at 1355 cm^{-1}, 1584 cm^{-1}, and 2715.6 cm^{-1} respectively, and a silicon peak at 519.4 cm^{-1}.

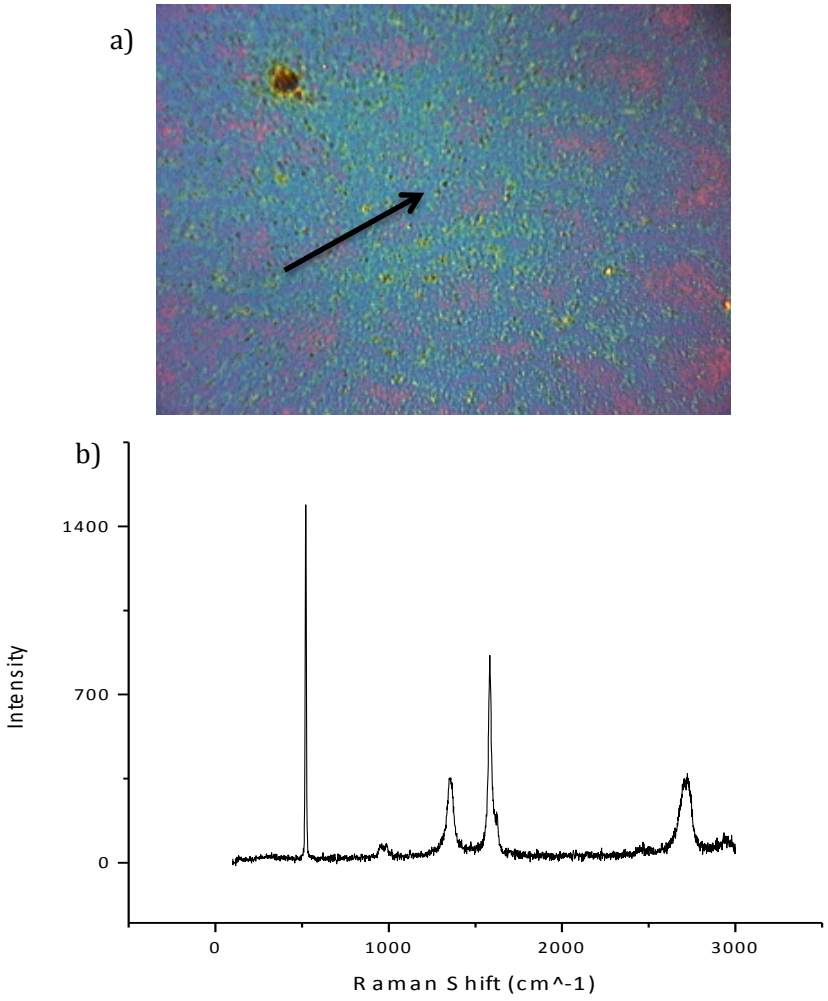

Figure 35: a) Optical image of the surface of SiO_2/Si spin coated with carbon solution and annealed at 200°C with the graphitic film appearing yellow, green, blue, or purple depending on its thickness and the bare substrate appearing pink. The tip of the arrow indicates where the Raman measurement was taken. b) Corresponding Raman spectrum showing clear D, G, and 2D peaks at 1358.5 cm^{-1}, 1582.5 cm^{-1}, and 2723.3 cm^{-1} respectively, and a silicon peak at 520.9 cm^{-1}. Notice the spectrum is not sloped upwards like the one observed from the sample where the nickel diffusion layer was applied.

As considered in the Raman Spectroscopy section of the preceding review, graphitic materials exhibit characteristic D, G, and 2D peaks at around 1350 cm^{-1}, 1580 cm^{-1}, and 2700 cm^{-1}, respectively. The G band is due to the doubly degenerate E_{2g} phonon mode at the Brillouin zone center and the 2D band is a result of second order zone boundary phonons and occurs at approximately twice the value of shift of the D band. Both bulk graphite and graphene show G and 2D peaks, however the 2D/G integrated intensity area ratio of graphene is much higher than that of graphite due to the more intense 2D peak with respect to the G peak. The D peak arises from atomic disorder and defects within the material, thus a decrease in the D/G integrated intensity area ratio signifies a reduction in the number of defects and an increase in the ratio signifies an escalation in the number of defects. Due to the substrate being SiO_2/Si, a peak at approximately 520 cm^{-1} corresponding to silicon is also expected.

For comparison, a control sample of just the carbon solution spin coated on a bare SiO_2/Si substrate and annealed at 200°C was also characterized. Its data is presented in Figure 35. Immediately, a significant difference between the Raman spectra of the control and those of the variable samples is evident: the existence of a positive slope increasing with Raman shift in all of the samples in which the nickel diffusion layer was applied. While the presence of the typical G, D, and 2D peaks confirms the material is graphitic, the increasing slope suggests that the nickel layer has not fully been etched off the samples and is inducing this gradual increase in Raman shift. Examination of the position of the 2D peaks shows no trend either within a certain sample or from sample to sample, indicating that there is no conclusive change in the number of graphitic layers within a sample or among samples treated with different annealing temperatures.

The areas under the D, G, and 2D peaks were also determined for both the etched samples on which diffusion through nickel took place and the control sample and compiled

into D/G and 2D/G integrated intensity area ratios. Plots of these ratios vs. temperature are portrayed in Figures 36 and 37. It is important to note that due to the lack of significant 2D peaks in the samples annealed at 400°C, those data points are not present on the 2D/G ratio plot. The 2D/G area ratio displays an increase in value until the 100° – 150°C range, then a decrease at 200°C. This could indicate the existence of films with fewer layers at 100° and 150°C as opposed to those annealed at 50° and 200°C, suggesting that the ideal growth temperature for few layer graphene annealed for 4 hours is somewhere within that 100° – 150°C range. The 2D/G ratio value for the control annealed carbon solution at 200°C is noticeably higher than those of the diffused carbon samples, which could signify that the control carbon is thinner than the graphitic films grown via diffusion through nickel.

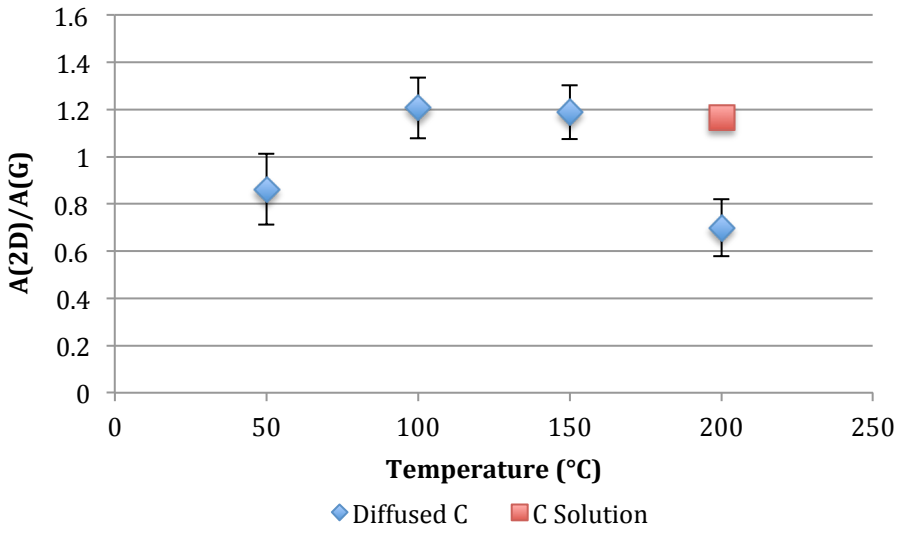

Figure 36: Plot of the 2D/G integrated intensity area ratio as a function of annealing temperature. Carbon diffused through nickel is indicated in blue and the control carbon solution is indicated in red. Note that due to the lack of significant 2D peaks in the samples annealed at 400°C, those data points are not presented on this plot.

Unlike the previous 2D/G ratio results, the D/G area ratio initially shows a slight decrease with respect to annealing temperature until around 150°C, suggesting a logical reduction of defects within the graphitic material as temperature increases. However, the

data then demonstrates a counterintuitive increase in D/G ratio with elevating temperature, indicating that disorder increases. The D/G ratio value for the control annealed carbon solution at 200°C falls directly within the range of the diffused carbon samples.

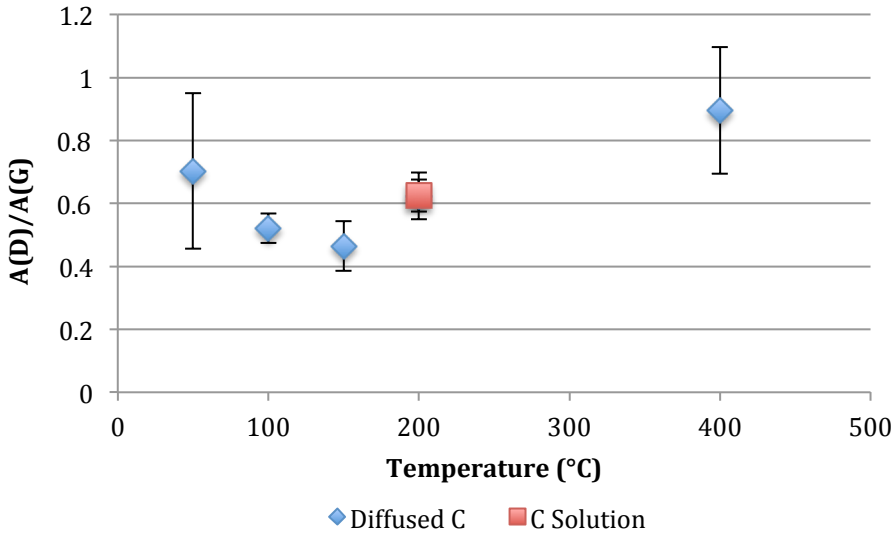

Figure 37: Plot of the D/G integrated intensity area ratio as a function of annealing temperature. Carbon diffused through nickel is indicated in blue and the control carbon solution is indicated in red.

Overall, the Raman data indicates that while there is graphitic material present on the diffused carbon samples, it is not monolayer or few layer graphene. This is most likely due to flaws in the experimental procedure, particularly the etching. Both the presence of a positive slope increasing with Raman shift and the direct overlapping of the D/G area ratio of the control annealed carbon solution with the range of the diffused carbon samples at 200°C suggest that the nickel diffusion layer was not successfully etched off, and thus the graphitic substance observed is just the original carbon solution. This fault could have arisen from either an ineffective etching solution, or the prospect that during the spin coating process, the carbon solution coated not only the top but the sides of the samples as well, completely sealing off the nickel layer and prohibiting exposure to the etchant.

Part II, Section IV – Conclusion

In summary, the main objective of this work was to establish a novel procedure for the synthesis of scalable, high quality graphene thin films onto insulating substrates that could be implemented on an industrial level. A procedure in which carbon from a solid source is diffused through a thin nickel layer directly onto an insulating substrate was proposed. This was achieved by thermal evaporation of a 40 nm layer of nickel onto a SiO_2/Si substrate, which was then spin coated with a carbon solution and annealed to initiate the diffusion of carbon into the metal. Once the carbon atoms travelled through the layer, they precipitated out at the interface between the nickel and the SiO_2/Si substrate, generating a graphene thin film. Specimens were annealed at 50°C, 100°C, 150°C, 200°C, or 400°C for 4 hours followed by submergence in an etchant to remove the metal layer and any excess carbon solution.

After preparation, Raman spectra and corresponding optical images were found and documented for different locations along the sample surfaces. Being a graphitic material, distinctive D, G, and 2D peaks at around 1350 cm^{-1}, 1580 cm^{-1}, and 2700 cm^{-1} and a silicon peak at approximately 520 cm^{-1} from the substrate were expected. The Raman spectra did prove that the material was graphitic, but an increasing slope in the Raman shift suggested that the nickel layer was still present. A study of the positions of the 2D peaks both within a specific sample and among all samples showed no conclusive trend. 2D/G area ratios displayed an increase in value as a function of annealing temperature until the 100° – 150°C range, then a decrease at 200°C. This could have indicated that the ideal nucleation and growth temperature for these experimental conditions was within that 100° – 150°C range. D/G area ratios showed a slight decrease with respect to annealing temperature until around 150°C, suggesting a logical reduction of defects. The data then exhibited a counterintuitive increase in D/G ratio, indicating that disorder increased.

It can be concluded from these results that there were flaws in this procedure preventing the diffused carbon from being properly observed and characterized. This is thought to have arisen from an inadequate etching process, preventing the nickel and excess carbon from being completely removed and thus masking the diffused graphene. Causes of this error could be due to an inappropriate etching solution, or the possibility that the carbon solution covered the sides of the samples during spin coating and prevented interaction between the nickel layer and the etchant.

Part II, Section V – Contemporary/Future Work

While unfortunately the previously discussed results weren't successful, Kwak et al has very recently proven that this technique is an effective route to growing transfer-free graphene on arbitrary substrates [44]. In their work, a 100 nm nickel layer was deposited on oxidized silicon, poly(methyl methacrylate) (PMMA) coated SiO_2, and commercially available glass substrates via electron beam evaporation. Nickel coatings on the SiO2/Si substrates were subsequently heat treated at ~1000°C in order to retexture the metal, forming grain sizes of approximately 5-20 μm as opposed to the initial 40-50 nm grain widths. These were then plastered with a carbon paste created by the dispersion of graphite powder in ethanol. In order to guarantee the contact between the nickel/carbon interface, a molybdenum holding stage was employed to clamp the samples at a pressure of less that 1 MPa. Annealing took place in a tube furnace at temperatures ranging from 25° to 260°C for 1 to 10 minutes, under an argon or an ambient air environment. The samples were then etched in an aqueous solution of iron(III) chloride ($FeCl_3$) to remove the metal and uncover the diffused graphene. The authors coined this method "diffusion-assisted synthesis", or DAS [44]. A schematic of this progression can be found in Figure 38.

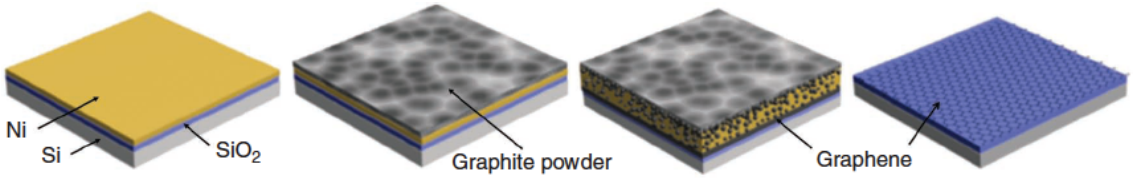

Figure 38: Schematic of the DAS procedure. Reprinted by permission from Macmillan Publishers Ltd: Nature Communications [44], copyright 2012.

Raman analysis of the samples grown on SiO_2/Si substrates revealed the existence of mono-, bi-, and trilayer graphene as evident in the optical image and Raman spectra displayed in Figure 39. Peaks at ~1351 cm^{-1}, ~1592 cm^{-1}, and ~2685 cm^{-1} resultant of the D, G, and 2D bands confirm that the material was indeed graphitic and indicated that low

defect graphene sheets were grown. Thicknesses were ascertained using G/2D intensity ratios and full width at half maximum (FWHM) measurements of the 2D peak. Visual examination of these films showed topologically smooth and wrinkle-free surfaces and correlation in morphologies between 1-2 layer thick areas and grains in the nickel layer. This provides evidence to the theory that nickel grain boundaries act as nucleation sites for diffused carbon. FET devices made with these graphene films demonstrated an estimated carrier mobility of ~667 $cm^2V^{-1}s^{-1}$ and a sheet resistance of ~1000 Ω/□, proving this material's potential to be employed as transparent conductive electrodes [44].

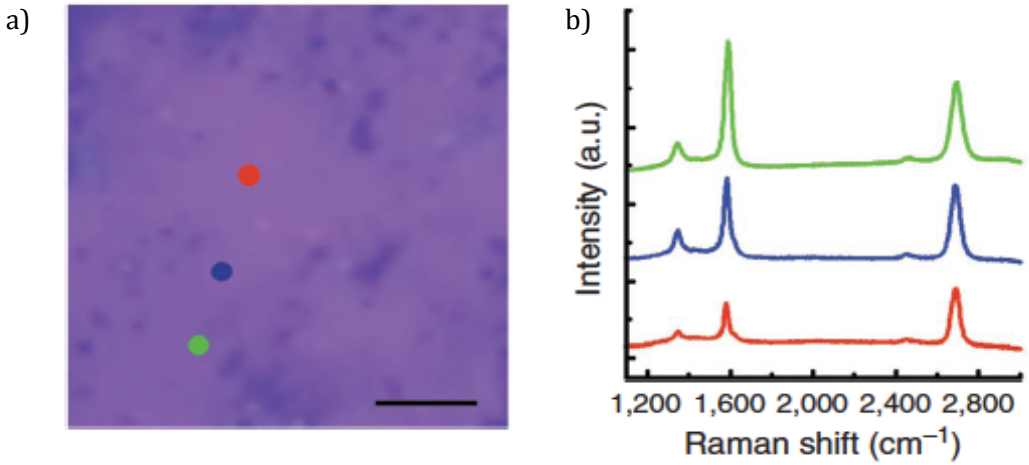

Figure 39: a) Optical image of a graphene film grown via nickel diffusion on a SiO_2/Si substrate annealed at 160°C for 5 minutes. b) Raman spectra from several locations on the previous optical images as indicated by the matching colors. The one layer spectrum appears in red, the two layer in blue, and the three layer in green. Reprinted by permission from Macmillan Publishers Ltd: Nature Communications [44], copyright 2012.

Upon comparison of graphene films produced under argon and those produced under air environments, there was surprisingly very little disparity in surface morphology, areal coverage, and Raman characteristics. Annealing temperature, however, did have an effect on growth conditions. Surface coverage increased from ~60 to ~98% as the temperature was elevated from 25° to 260°C. The authors noted that continuous sheets could only be achieved at temperatures at or above 160°C. Studies of G/2D intensity ratios

and FWHM of G bands were also performed and it was concluded that the quality of the graphene films stayed consistent despite the variable annealing temperatures [44].

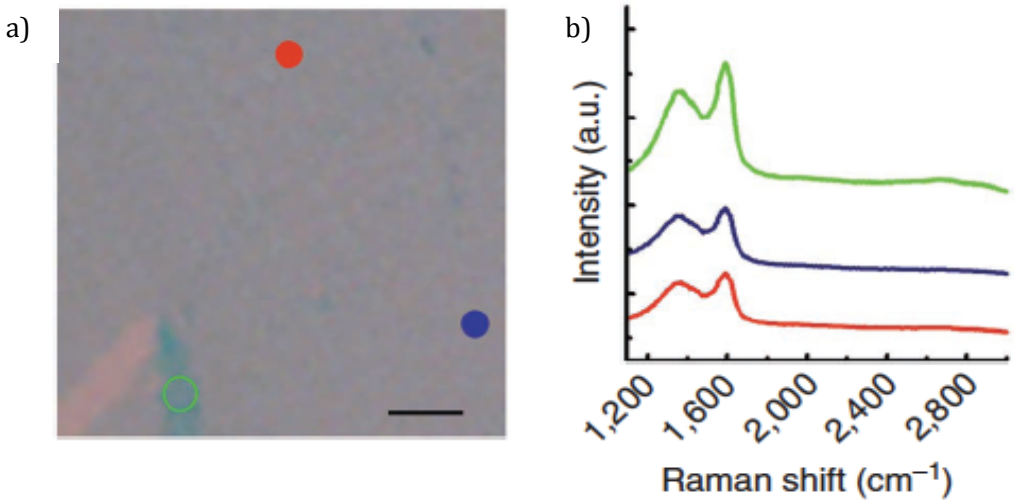

Figure 40: a) Optical image of a graphene film grown via nickel diffusion on PMMA annealed at 60°C for 10 minutes, then transferred to a SiO_2/Si substrate. b) Raman spectra from several locations on the previous optical images as indicated by the matching colors. The one layer spectrum appears in red, the two layer in blue, and the three layer in green. Reprinted by permission from Macmillan Publishers Ltd: Nature Communications [44], copyright 2012.

As opposed to the films found on the SiO_2/Si substrates, Raman characterization of the material grown on the PMMA/SiO_2 and glass substrates indicated that a different type of graphitic material was generated. An example of an optical image and Raman spectra of one of these samples is presented in Figure 40. These spectra exhibited a D peak at 1359±4 cm^{-1} and a G peak at 1594±2 cm^{-1} along with sizeable FWHMs and D/G intensity ratios larger than those of the graphene produced on SiO_2/Si substrates, all of which were characteristic of nanocrystalline graphene. Areas of continuous graphitic material were evident on PMMA and glass substrates annealed at all different temperatures, which the authors suggested was a result of the small grain size in the nickel diffusion layer [44].

It was proposed that the nanocrystalline films were formed via the second carbon diffusion mechanism discussed in the Introduction/Background, in which carbon atoms

homogeneously nucleate at various locations along the substrate surface. Instead of arising from supersaturation of the diffusion layer as was stated previously, this is most likely to have occurred from more densely populated grain boundaries in the nickel. Graphene films grown on the SiO_2/Si substrates with more spread apart grain boundaries occurred via the first mechanism, where carbon migrates to the grain boundaries and heterogeneously nucleates into graphene layers that propagate outward along the nickel grain [44]. Figure 41 portrays a schematic illustration of both of these mechanisms for the diffusion of carbon through nickel onto the substrate surface.

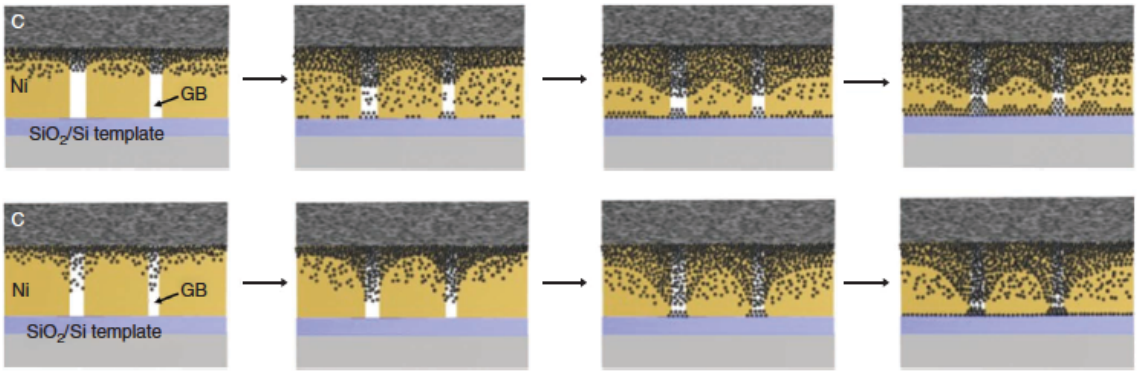

Figure 41: Schematic of two possible mechanisms for the DAS process. Reprinted by permission from Macmillan Publishers Ltd: Nature Communications [44], copyright 2012.

Overall, the Kwak et al article was successful in proving that high quality graphene thin films a) can be grown via diffusion through nickel onto arbitrary substrates and b) have the potential to be employed for industrial use. Several key differences exist between their work and the experiment presented in this thesis that could be the reason behind the varying outcomes. First, the term "plastered" when compared to "spin coated" suggests that they utilized more carbon paste on a given sample and that the carbon did not conceal the sides of the substrate, which was thought to have posed a problem with the proposed etching procedure. Second, they deposited a much thicker 100 nm layer of nickel that absorbed all of the carbon paste upon annealing, unlike the 40 nm layer utilized previously.

They also subjected their nickel layers on SiO_2/Si substrates to a heat treatment to reform the grains and reestablish their boundaries, resulting in grain sizes that most likely much larger than the ones present in the previous experiment.

Future work in this area could include the following: better grain boundary engineering to control structural and electronic properties of the material given that these are the nucleation sites for the diffused carbon atoms, exploration of different types of carbon source solutions and how they are applied, variation of the thickness of the nickel diffusion layer, applications of graphene through diffusion onto a wider range of substrates, and implementation of other high carbon solubility metals, such as cobalt. In conclusion, this straightforward, low temperature technique for growing large-area graphene is not only effective, but also has the potential to revolutionize the industry of electronic and optoelectronic devices.

Bibliography

[1] Singh, V., Joung, D., Zhai, L., Das, S., Khondaker, S. I., & Seal, S. Graphene based materials: Past, present, and future. *Progress in Materials Science* **56**, 1178-1271 (2011).

[2] Geim, A. K. & Novoselo, K. S. The rise of graphene. *Nature Materials* **6**, 183-191 (2007).

[3] Hancock, Y. The 2010 Noble Prize in physics – ground-breaking experiments on graphene. *Journal of Physics D: Applied Physics* **44**, 473001 (2011).

[4] Novoselov, K. S., Jiang, D., Schedin, F., Khotkevich, V. V., Morozov, S. V., & Geim, A. K. Two-dimensional atomic crystals. *PNAS* **102**, 10451-10453 (2005).

[5] Boehm, H. P., Setton, R., & Stumpp, E. Nomenclature and Terminology of Graphite Intercalation Compounds. *Pure and Applied Chemistry* **66**, 1893-1901 (1994).

[6] Novoselov, K. S., Geim, A. K., Morozov, S. V., Jiang, D., Zhang, Y., Dubonos, S. V., Grigorieva, I. V., & Firsov, A. A. Electric Field Effect in Atomically Thin Carbon Films. *Science* **306**, 666-669 (2004).

[7] Hernandez, Y., Nicolosi, V., Lotya, M., Blighe, F. M., Sun, Z., De, S., McGovern, I. T., Holland, B., Bryne, M., Gun'ko, Y. K., Boland, J. J., Niraj, P., Duesberg, G., Krishnamurthy, S., Goodhue, R., Hutchinson, J., Scardaci, V., Ferrari, A. C., & Coleman, J. N. High-yield production of graphene by liquid-phase exfoliation of graphite. *Nature Nanotechnology* **3**, 563-568 (2008).

[8] Lotya, M., Hernandez, Y., King, P. J., Smith, R. J., Nicolosi, V., Karlsson, L. S., Blighe, F. M., De, S., Wang, Z., McGovern, I. T., Duesberg, G. S., & Coleman, J. N. Liquid Phase Production of Graphene by Exfoliation in Surfactant/Water Solutions. *Journal of the American Chemical Society* **131**, 3611-3620 (2009).

[9] Green, A. A. & Hersam, M. C. Solution Phase Production of Graphene with Controlled Thickness via Density Differentiation. *Nano Letters* **9**, 4031-4036 (2009).

[10] Reina, A., Jia. X., Ho, J., Son, H., Bulovic, V., Dresselhaus, M. S., & Kong, J. Large Area, Few-Layer Graphene Films on Arbitrary Substrates by Chemical Vapor Deposition. *Nano Letters* **9**, 30-35 (2009).

[11] Li, X., Cai, W., An, J., Kim, S., Nah, J., Yang, D., Piner, R., Velamakanni, A., Jung, I., Tutuc, E., Banerjee, S. K., Colombo, L., & Ruoff, R. S. Large-Area Synthesis of High-Quality and Uniform Graphene Films on Copper Foils. *Science* **324**, 1312-1314 (2009).

[12] Zhu, Y., Murali, S., Cai, W., Li, X., Suk, J. W., Potts, J. R., & Ruoff, R. S. Graphene and Graphene Oxide: Synthesis, Properties, and Applications. *Advanced Materials* **22**, 3906-3924 (2010).

[13] Malesevic, A., Vitchev, R., Schouteden, K., Volodin, A., Zhang, L., Van Tendeloo, G., Vanhulsel, A., & Van Haesendonck, C. Synthesis of few-layer graphene via microwave plasma-enhanced chemical vapour deposition. *Nanotechnology* **19**, 305604 (2008).

[14] Berger, C., Song, Z., Li, T., Li, X., Ogbazghi, A. Y., Fang, R., Dai, Z., Marchenkov, A. N., Conrad, E. H., First, P. N., & de Heer, W. A. Ultrathin Epitaxial Graphite: 2D Electron Gas Properties and a Route toward Graphene-based Nanoelectronics. *Journal of Physical Chemistry B* **108**, 19912-19916 (2004).

[15] Sutter, P. W., Flege, J. I., & Sutter, E. A. Epitaxial graphene on ruthenium. *Nature Materials* **7**, 406-411 (2008).

[16] Eda, G. & Chhowlla, M. Chemically Derived Graphene Oxide: Towards Large-Area Thin-Film Electronics and Optoelectronics. *Advanced Materials* **22**, 2392-2415 (2010).

[17] Lerf, A., He, H., Forster, M., & Klinowski, J. Structure of Graphite Oxide Revisited. *Journal of Physical Chemistry B* **102**, 4477-4482 (1998).

[18] Erickson, K., Erni, R., Lee, Z., Alem, N., Gannett, W., & Zettl, A. Determination of the Local Chemical Structure of Graphene Oxide and Reduced Graphene Oxide. *Advanced Materials* **22**, 4467-4472 (2010).

[19] Li, X., Wang, X., Zhang, L., Lee, S., & Dai, H. Chemically Derived, Ultrasmooth Graphene Nanoribbon Semiconductors. *Science* **319**, 1229-1232 (2008).

[20] Kosynkin, D. V., Higginbotham, A. L., Sinitskii, A., Lomeda, J. R., Dimiev, A., Price, B. K., & Tour, J. M. Longitudinal unzipping of carbon nanotubes to form graphene nanoribbons. *Nature* **458**, 872-876 (2009).

[21] Blake, P., Hill, E. W., Castro Neto, A. H., Novoselov, K. S., Jiang, D., Yang, R., Booth, T. J., & Geim, A. K. Making graphene visible. *Applied Physics Letters* **91**, 063124 (2007).

[22] Paredes, J. I., Solís-Fernández, P., Martínez-Alonso, A., & Tascón, J. M.D. Atomic Force and Scanning Tunneling Microscopy Imaging of Graphene Nanosheets Derived from Graphite Oxide. *Langmuir* **25**, 5957-5968 (2009).

[23] Girit, C. O., Meyer, J. C., Erni, R., Rossell, M. D., Kisielowski, C., Yang, L., Park, C. H., Crommie, M. F., Cohen, M. L., Louie, S. G., & Zettl, A. Graphene at the Edge: Stability and Dynamics. *Science* **323**, 1705-1708 (2009).

[24] Meyer, J. C., Kisielowski, C., Erni, R., Rossell, M. D., Crommie, M. F., & Zettl, A. Direct Imaging of Lattice Atoms and Topological Defects in Graphene Membranes. *Nano Letters* **8**, 3582-3586 (2008).

[25] Gómez-Navarro, C., Meyer, J. C., Sundaram, R. S., Chuvilin, A., Kurasch, S., Burghard, M., Kern, K., & Kaiser, U. Atomic Structure of Reduced Graphene Oxide. *Nano Letters* **10**, 1144-1148 (2010).

[26] Gass, M. H., Bangert, U., Bleloch, A. L., Wang, P., Nair, R. R., & Geim, A. K. Free-standing graphene at atomic resolution. *Nature Nanotechnology* **3**, 676-681 (2008).

[27] Ferrari, A. C., Meyer, J. C., Scardaci, V., Casiraghi, C., Lazzeri, M., Mauri, F., Piscanec, S., Jiang, D., Novoselov, K. S., Roth, S., & Geim, A. K. Raman Spectrum of Graphene and Graphene Layers. *Physical Review Letters* **97**, 187401 (2006).

[28] Kim, J. Cote, L. J., Kim, F., & Huang, J. Visualizing Graphene Based Sheets by Fluorescence Quenching Microscopy. *Journal of the American Chemical Society* **132**, 260-267 (2010).

[29] Wu, Y. H, Yu. T., & Shen, Z. X. Two-dimensional carbon nanostructures: Fundamental properties, synthesis, characterization, and potential applications. *Journal of Applied Physics* **108**, 071301 (2010).

[30] Fasolino, A., Los, J. H., & Katsnelson, M. I. Intrinsic ripples in graphene. *Nature Materials* **6**, 858-861 (2007).

[31] Novoselov, K. S., Geim, A. K., Morosov, S. V., Jiang, D., Katsnelson, M. I., Grigorieva, I. V., Dubonos, S. V., & Firsov, A. A. Two-dimensional gas of massless Dirac fermions in graphene. *Nature* **438**, 197-200 (2005).

[32] Bonaccorso, F., Sun, Z., Hasan, T., & Ferrari, A. C. Graphene photonics and optoelectronics. *Nature Photonics* **4**, 611-622 (2010).

[33] Nair, R. R., Blake, P., Grigorenko, A. N., Novoselov, K. S., Booth, T. J., Stauber, T., Peres, N. M. R., & Geim, A. K. Fine Structure Constant Defines Visual Transparency of Graphene. *Science* **320**, 1308 (2008).

[34] Lee, C., Wei, X., Kysar, J. W., & Hone, J. Measurement of the Elastic Properties and Intrinsic Strength of Monolayer Graphene. *Science* **321**, 385-388 (2008).

[35] Kim, K. S., Zhao, Y., Jang, H., Lee, S. Y., Kim, J. M., Kim, K. S., Ahn, J. H., Kim, P., Choi, J. Y., & Hong, B. H. Large-scale pattern growth of graphene films for stretchable transparent electrodes. *Nature* **457**, 706-710 (2009).

[36] Balandin, A. A., Ghosh, S., Bao, W., Calizo, I., Teweldebrhan, D., Miao, F., & Lau, C. N. Superior Conductivity of Single-Layer Graphene. *Nano Letters* **8**, 902-907 (2008).

[37] Choi, W., Lahiri, I., Seelaboyina, R., & Kang, Y. S. Synthesis of Graphene and Its Applications: A Review. *Critical Reviews in Solid State and Materials Sciences* **35**, 52-71 (2010).

[38] Wang, X., Zhi, L., and Mullen, K. Transparent, Conductive Graphene Electrodes for Dye-Sensitized Solar Cells. *Nano Letters* **8**, 323-327 (2008).

[39] Fowler, J. D., Allen, M. J., Tung, V. C., Yang, Y., Kaner, R. B., & Weiller, B. H. Practical Chemical Sensors from Chemically Derived Graphene. *ACS Nano* **3**, 301-306 (2009).

[40] Paek, S. M., Yoo, E., Honma, I. Enhanced Cyclic Performance and Lithium Storage Capacity of SnO_2/Graphene Nanoporous Electrodes with Three-Dimensionally Delaminated Flexible Structure. *Nano Letters* **9**, 72-75 (2009).

[41] Chen, Z., Li, Y. M., Rooks, M. J., and Avouris, P. Graphene nano-ribbon electronics. *Physica E* **40**, 228-232 (2007).

[42] Baraton, L., He, Z. B., Lee, C. S., Cojocaru, C. S., Châtelet, M., Maurice, J. L., Lee, Y. H., & Pribat, D. On the mechanisms of precipitation of graphene on nickel thin films. *EPL* **96**, 46003 (2011).

[43] Lander, J. J., Kern, H. E., & Beach, A. L. Solubility and Diffusion Coefficient of Carbon in Nickel: Reaction Rates of Nickel-Carbon Alloys with Barium Oxide. *Journal of Applied Physics* **23**, 1305-1309 (1952).

[44] Kwak, J., Chu, J. H., Choi, J. K., Park, S. D., Go, H., Kim, S. Y., Park, K., Kim, S. D., Kim, Y. W., Yoon, E., Kodambaka, S., & Kwon, S. Y. Near room-temperature synthesis of transfer-free graphene films. *Nature Communications* **3**, (2012).